



HAL
open science

Intracellular Distribution of Manganese by the Trans-Golgi Network Transporter NRAMP2 Is Critical for Photosynthesis and Cellular Redox Homeostasis

Santiago Alejandro, Rémy Cailliatte, Carine Alcon, Leon Dirick, Frédéric Domergue, David Correia, Loren Castaings, Jean-Francois Briat, Stephane Mari, Catherine Curie

► To cite this version:

Santiago Alejandro, Rémy Cailliatte, Carine Alcon, Leon Dirick, Frédéric Domergue, et al.. Intracellular Distribution of Manganese by the Trans-Golgi Network Transporter NRAMP2 Is Critical for Photosynthesis and Cellular Redox Homeostasis. *The Plant cell*, 2017, 29 (12), pp.3068-3084. 10.1105/tpc.17.00578 . hal-01695892

HAL Id: hal-01695892

<https://hal.science/hal-01695892>

Submitted on 18 Dec 2020

HAL is a multi-disciplinary open access archive for the deposit and dissemination of scientific research documents, whether they are published or not. The documents may come from teaching and research institutions in France or abroad, or from public or private research centers.

L'archive ouverte pluridisciplinaire **HAL**, est destinée au dépôt et à la diffusion de documents scientifiques de niveau recherche, publiés ou non, émanant des établissements d'enseignement et de recherche français ou étrangers, des laboratoires publics ou privés.

RESEARCH ARTICLE

**Intracellular Distribution of Manganese by the Trans-Golgi Network
Transporter NRAMP2 is Critical for Photosynthesis and Cellular Redox
Homeostasis**

Santiago Alejandro*, **Rémy Cailliatte***, **Carine Alcon**, **Léon Dirick**, **Frédéric Domergue¹**,
David Correia, **Loren Castaings**, **Jean-François Briat**, **Stéphane Mari** and **Catherine
Curie²**

BPMP, CNRS, INRA, Montpellier SupAgro, Univ Montpellier, Montpellier, France.

¹Laboratoire de Biogénèse Membranaire CNRS - Université de Bordeaux - UMR 5200, Villenave d'Ornon, France.

* S.A. and R.C. contributed equally to this work

²Corresponding Author: catherine.curie@cnrs.fr

Short title: Intracellular distribution of Mn by NRAMP2

One sentence summary: The metal transporter NRAMP2 controls photosynthesis and antioxidant defenses by releasing manganese from the trans-Golgi network, thus building up a cytosolic pool that feeds downstream organelles.

The author responsible for distribution of materials integral to the findings presented in this article in accordance with the policy described in the Instructions for Authors (www.plantcell.org) is: Catherine Curie (catherine.curie@cnrs.fr)

ABSTRACT

Plants require trace levels of manganese (Mn) for survival, as it is an essential cofactor in oxygen metabolism, especially O₂ production via photosynthesis and the disposal of superoxide radicals. These processes occur in specialized organelles, requiring membrane-bound intracellular transporters to partition Mn between cell compartments. We identified an *Arabidopsis thaliana* member of the NRAMP family of divalent metal transporters, NRAMP2, which functions in the intracellular distribution of Mn. Two knockdown alleles of NRAMP2 showed decreased activity of photosystem II and increased oxidative stress under Mn-deficient conditions, yet total Mn content remained unchanged. At the subcellular level, these phenotypes were associated with a loss of Mn content in vacuoles and chloroplasts. NRAMP2 was able to rescue the mitochondrial yeast mutant *mtm1Δ*. In plants, NRAMP2 is a resident protein of the trans Golgi network. NRAMP2 may act indirectly on downstream organelles by building up a cytosolic pool that is used to feed target compartments. Moreover, not only does the *nramp2* mutant accumulate superoxide ions, but NRAMP2 can functionally replace cytosolic superoxide dismutase in yeast, indicating that the pool of Mn displaced by NRAMP2 is required for the detoxification of reactive oxygen species.

1 INTRODUCTION

2 Mn serves as a cofactor for an array of enzymes and pathways, the most important of which is
3 the antioxidant defense enzyme manganese superoxide dismutase (Mn SOD), which
4 dismutates superoxide anion into the less toxic hydrogen peroxide and oxygen in
5 mitochondria and peroxisomes (del Rio et al., 2003). In addition, photosynthetic organisms
6 use Mn in the reaction center of photosystem II (PSII), in which a four Mn-cluster coordinates
7 with the oxygen evolving complex to perform the water-splitting reaction (Nickelsen and
8 Rengstl, 2013). For these reasons, Mn deficiency in plants targets two essential cellular
9 functions: antioxidant capacity and photosynthetic activity. Although Mn is rarely limiting for
10 animal cells, its bioavailability to plants is dramatically reduced in dry, well-aerated and
11 alkaline soils, which negatively affects plant growth. Visual symptoms of Mn shortage are
12 limited to young leaves, which are chlorotic at moderate deficiency but develop necrosis at
13 extreme deficiency levels (Schmidt et al., 2016). Consequently, the agronomical
14 repercussions of Mn deficiency have been underestimated and the molecular mechanisms at
15 work in the response to Mn limitation have been little explored compared to those of other
16 essential metals such as Fe, Zn and Cu. Mn excess can also be detrimental to organisms. Mn
17 toxicity leads to a predisposition to genomic instability (Garcia-Rodriguez et al., 2012) and
18 causes a neurological syndrome in human called manganism, with symptoms resembling
19 those of Parkinson disease (Roth, 2006). In plants, Mn toxicity is widespread in acidic soils,
20 where it becomes more available and provokes quite diverse symptoms often characterized by
21 brown speckles containing oxidized Mn on mature leaves and/or interveinal chlorosis and
22 necrosis (Marschner et al., 1986).

23 Most species acquire Mn via transporters of the Natural Resistance-Associated
24 Macrophage protein (NRAMP) family. These divalent metal/proton symporters harbor a
25 broad range specificity for metals (Nevo and Nelson, 2006). In *Arabidopsis thaliana* and rice
26 (*Oryza sativa*), high-affinity Mn uptake in root depends on the presence of NRAMP1 and
27 NRAMP5, respectively, at the root surface. Loss-of-function of *Arabidopsis NRAMP1* or rice
28 *NRAMP5* dramatically decreases the tolerance of the plant to Mn deficiency (Cailliatte et al.,
29 2010; Ishimaru et al., 2012; Sasaki et al., 2012). These proteins are therefore true orthologs of
30 the NRAMP transporter Smf1p in yeast (Cohen et al., 2000). Moreover, in most species, Mn
31 is a substrate of the high affinity, root-surface-localized Fe uptake transporter IRT1, which
32 was shown in *Arabidopsis* to contribute to Mn acquisition when combined with the *nramp1*
33 mutation (Castaings et al., 2016).

34 Our understanding of the mechanisms of the intracellular distribution of Mn is still
35 fragmentary. In plants, trafficking of Mn across the membranes of major organelles is

36 mediated by transporters belonging to a variety of transporter families. In seeds, the
37 tonoplasmic VIT1 transporter mediates import of Mn and Fe into the vacuole (Kim et al., 2006;
38 Momonoi et al., 2009; Zhang et al., 2012) from where these metals are remobilized in
39 Arabidopsis by the NRAMP transporters NRAMP3 and NRAMP4. By mediating Mn efflux
40 from the vacuole, these two highly homologous tonoplasmic proteins help maintain efficient
41 PSII activity under Mn-limiting conditions (Lanquar et al., 2005; Lanquar et al., 2010). Mn
42 vacuolar transporters also include i) CAX2, a Ca^{2+} /cation antiporter involved in the vacuolar
43 sequestration of Mn (Pittman et al., 2004); ii) ZIP1, a homolog of IRT1 located within the
44 tonoplast membrane of root stele cells, where it is thought to participate in the remobilization
45 of Mn from the vacuole to the cytosol and mediate radial movement of Mn in the root (Milner
46 et al., 2013); and iii) METAL TOLERANT PROTEIN8 members in rice (Os-MTP8.1) and
47 Arabidopsis (MTP8), which belong to the subgroup of cation diffusion facilitators (CDF)
48 involved in proton/Mn antiport that help protect the cell from Mn toxicity by targeting excess
49 cytosolic Mn to the vacuole (Eroglu et al., 2016). How Mn is transported into mitochondria is
50 currently unknown. A study in yeast (*Saccharomyces cerevisiae*) initially identified the
51 Mtm1p carrier as the Mn importer into the mitochondrial matrix because its inactivation led to
52 reduced Mn SOD activity and was rescued by supplying the cells with a large amount of Mn
53 (Luk et al., 2003). However, the function of Mtm1p was subsequently reassigned to the
54 control of mitochondrial Fe homeostasis via the import of an enzymatic cofactor that plays a
55 key role in heme biosynthesis (Whittaker et al., 2015). Because the yeast Mtm1p mutant
56 *mtm1Δ* accumulates Fe in its mitochondria, mis-metallation of SOD2 occurs, leading to its
57 inactivation unless the cells are treated with high levels of Mn (Yang et al., 2006). At-MTM1,
58 a likely ortholog of Mtm1p, has been identified in Arabidopsis (Su et al., 2007). No Mn
59 transporter has yet been identified on the chloroplast envelope, but a thylakoid transporter has
60 recently been reported. PHOTOSYNTHESIS AFFECTED MUTANT71 (PAM71) is required
61 for the incorporation of Mn into the oxygen evolving complex of PSII, presumably by
62 transporting Mn into the thylakoid lumen (Schneider et al., 2016).

63 Mn trafficking into the secretory pathway appears to fulfill important functions in
64 maintaining Mn homeostasis in all kingdoms. Members of the $\text{P}_{2\text{A}}$ -type ATPase family were
65 shown to function as $\text{Ca}^{2+}/\text{Mn}^{2+}$ pumps in several organisms. Among these, yeast Pmr1p
66 transports Mn into Golgi-like compartments and its inactivation leads to Mn accumulation in
67 the cytosol, causing Mn toxicity (Rudolph et al., 1989). Two Pmr1p homologs in Arabidopsis,
68 ECA1 and ECA3, which are located in the endoplasmic reticulum (ER) and Golgi,
69 respectively, can rescue *pmr1Δ* growth defect under Mn stress. Inactivation of *ECA1* and

70 *ECA3* alters the tolerance of plants to suboptimal Mn conditions (Wu et al., 2002; Mills et al.,
71 2008). Moreover, MTP11, another Mn-CDF member from Arabidopsis, and its barley
72 homolog Hv-MTP8, are localized in Golgi /PVC compartments where they control plant
73 tolerance to high Mn through a mechanism that may involve vesicular trafficking to the
74 vacuole and/or secretion to the extracellular space (Delhaize et al., 2007; Peiter et al., 2007;
75 Pedas et al., 2014). Finally, Smf2p, an NRAMP family transporter, is also present in the
76 secretory pathway in yeast, although its target compartment (reported as being intracellular
77 vesicles) still awaits formal identification (Luk and Culotta, 2001). Since Smf2p is required
78 for the activity of Sod2p and protein glycosylation, two enzymes that require a Mn cofactor,
79 this transporter was proposed to function in feeding Mn to downstream organelles (Luk and
80 Culotta, 2001).

81 Among the six NRAMP family members in Arabidopsis, NRAMP1, NRAMP3 and
82 NRAMP4 have been assigned a function in Mn or Mn/Fe transport (Curie et al., 2000;
83 Thomine et al., 2000; Lanquar et al., 2005; Cailliatte et al., 2010; Lanquar et al., 2010;
84 Castaings et al., 2016). A fourth member, NRAMP6, has been described as being able to
85 transport Cd, but its physiological function is currently unclear (Cailliatte et al., 2009). In this
86 study, through reverse genetics and functional complementation of yeast mutants, we show
87 that NRAMP2 is an important player in the Mn nutritional pathway in Arabidopsis. Its
88 presence in the endomembrane system is required for adequate distribution of Mn between
89 cell compartments, which is crucial for optimal PSII activity and for controlling reactive
90 oxygen species (ROS) production.

91

92

93 **RESULTS**

94

95 ***NRAMP2* knock-down mutants are hypersensitive to Mn deficiency**

96 To investigate the role of NRAMP2 in Arabidopsis, we used a reverse genetics
97 approach and analyzed a T-DNA insertion mutant line named *nramp2-3* (Figure 1). *NRAMP2*
98 transcript levels in the mutant line, as measured by quantitative RT-PCR, were strongly
99 reduced but still retained at 5 to 10% of wild-type levels, indicating that *nramp2-3* is a weak
100 allele of *NRAMP2* (Figure 1A,B). A second mutant allele of *NRAMP2*, named *nramp2-4*,
101 showed 40% residual *NRAMP2* transcript levels (Figure 1A,B). Therefore, both *nramp2-3* and
102 *nramp2-4* are knock-down alleles of *NRAMP2*. Since NRAMP family members have been
103 selected throughout evolution to transport Fe, Mn, or both, we searched for Fe and/or Mn

104 homeostasis defects in the *nramp2* mutants. Fe-limited or excess conditions did not affect the
105 growth of the *nramp2* mutants. In contrast, Mn limitation significantly altered the growth of
106 *nramp2-3*, and to a lesser extent that of *nramp2-4* (Figure 1C, Supplemental Figure 1A,B),
107 affecting the root more than the shoot (Figures 1D,E). Mn-deficient *nramp2-3* plants harbored
108 moderately chlorotic leaves (Figure 1C, Supplemental Figure 1A,B,D). Measurement of the
109 leaf SPAD index revealed a 44% reduction in chlorophyll content in Mn-deficient *nramp2-3*
110 plants (Supplemental Figure 1C). Mn addition to the hydroponic solution rescued the growth
111 defect of *nramp2-3* and partially restored its chlorophyll content (Figure 1D,E; Supplemental
112 Figure 1C,D). Complemented *nramp2* lines were generated by overexpressing a GFP-tagged
113 version of *NRAMP2* under the control of the *UBIQUITIN10* promoter (*ProUB10:NRAMP2-*
114 *GFP*) in the *nramp2-3* mutant background (Figure 1B). Two of the complemented lines
115 obtained, named OxNR2 #3 and OxNR2 #6, which overexpressed *NRAMP2* 12- and 8-fold,
116 respectively (Figure 1B), showed full reversion of the *nramp2-3* phenotype in Mn-deficient
117 growth conditions (Figure 1C-E). Altogether, these data demonstrate that decreasing
118 *NRAMP2* expression results in hypersensitivity of the plant to Mn deficiency, which suggests
119 that *NRAMP2* plays a role in Mn homeostasis.

120 We next measured Mn contents in shoots and roots of the *nramp2-3* mutant and
121 complemented lines (Figure 2). Under Mn replete conditions, both mutant and overexpressor
122 lines accumulated significantly higher levels of Mn in shoots and roots than wild type
123 (Supplemental Table 1). Upon Mn shortage, Mn levels in the tissues of the mutant were not
124 reduced. Instead, the Mn content increased by 26% in shoots of the *nramp2-3* mutant, a defect
125 that was fully rescued in the two complemented lines (Figure 2, Supplemental Table 1). This
126 result therefore ruled out the possibility that *NRAMP2* functions in the acquisition of Mn
127 from the growth medium. We next tested whether an increase in *NRAMP1* expression in roots
128 could account for the high level of Mn in the *nramp2-3* mutant subjected to Mn deficiency.
129 The accumulation of *NRAMP1* transcripts, however, was not significantly modified in
130 *nramp2-3* roots in response to Mn-deficiency (Supplemental Figure 2).

131

132 **NRAMP2 expression is ubiquitous in the plant**

133 We previously showed that *NRAMP2* is expressed in roots and to a lesser extent in shoots
134 (Curie et al., 2000). To examine the response of *NRAMP2* to Mn nutrition, plants were grown
135 in hydroponic conditions for 4 weeks including, or not, a 3-week period of Mn deficiency
136 (Figure 3). The results confirmed the higher accumulation of *NRAMP2* transcripts in roots

137 (Figure 3A). Moreover, the expression of *NRAMP2* was induced approximately 2.5-fold in
138 response to Mn deficiency both in roots and shoots compared to the control (Figure 3A).

139 To assess more precisely the localization of *NRAMP2* expression in plant tissues, we
140 generated transgenic plants carrying the β -glucuronidase (GUS) reporter gene under the
141 control of the *NRAMP2* promoter. Histochemical analysis of GUS activity showed staining in
142 vascular tissues of roots, cotyledons and leaves as well as in trichomes of young aerial tissues
143 (Figure 3B, panels a-c). In roots, staining was restricted to the stele, initiating in the
144 elongation zone and strengthening in older parts of the root (Figure 3B, panel d). Cross
145 sections through the root revealed preferential expression in the pericycle (Figure 3B, panel
146 e). In addition, transcriptional profiling in isolated root cell layers (Dinneny et al., 2008) also
147 revealed lower but significant *NRAMP2* expression in epidermis and cortex, particularly close
148 to the root tip (<http://www.bar.utoronto.ca/efp/cgi-bin/efpWeb.cgi>).

149

150 **NRAMP2 is localized in the TGN compartment**

151 In order to identify the target membrane of NRAMP2, we investigated the localization of
152 NRAMP2-GFP in complemented lines OxNR2 #3 and #6 expressing *ProUBI10:NRAMP2-*
153 *GFP* (Figure 4). GFP fluorescence, as observed by confocal imaging of root cells of 5-day-old
154 plants, appeared as dot-like structures throughout the cytoplasm, with no labeling of the
155 plasma membrane, which was exclusively labeled with the endocytic tracer FM4-64 (Figure
156 4A). This fluorescence pattern was unchanged under different Mn regimes. Kinetic analysis
157 of the uptake of FM4-64 revealed partial co-localization of FM4-64 with NRAMP2-GFP after
158 15 min of treatment (Figure 4B), thus indicating that NRAMP2 localizes to the
159 endomembrane system. To identify the compartment labeled by NRAMP2-GFP,
160 *ProUBI10:NRAMP2-GFP* was co-expressed with a set of organelle markers either by transient
161 expression in tobacco (*Nicotiana tabacum*) or through outcrossing with stably transformed
162 Arabidopsis marker lines. The two expression systems produced an identical pattern of
163 fluorescence for NRAMP2-GFP (Supplemental Figure 3A,B). No significant co-localization
164 was observed between NRAMP2-GFP and the peroxisomal marker px-rk CD3-983
165 (Supplemental Figure 3C,F). NRAMP2-GFP co-localized partially with the Golgi marker
166 SYP32 (Supplemental Figure 3D,G), and with the endosomal marker Rab A1g (Supplemental
167 Figure 3E,H).

168 To narrow down the localization of NRAMP2 within the endomembrane system,
169 *ProUBI10:NRAMP2-GFP* was co-expressed with markers of subcompartments of the Golgi
170 apparatus in tobacco leaves. NRAMP2-GFP was in all instances closely associated, - but

171 never co-localized -, with cis- and trans-Golgi markers ERD2 and Sialyl transferase (ST),
172 respectively (Figure 4C). Since NRAMP2-GFP was systematically distal to the ST-RFP trans-
173 Golgi marker (Figure 4C), we suspected that it was localized to the trans-Golgi Network
174 (TGN) compartment. Indeed, NRAMP2-GFP showed near-perfect co-localization with the
175 TGN marker SYP61-RFP (Figure 4D). Pearson correlation coefficients and Mander's overlap
176 coefficients above thresholds were calculated for NRAMP2-GFP with either the marker
177 ERD2-CFP, ST-RFP or RFP-SYP61 and confirmed the overlap between NRAMP2 and
178 SYP61 proteins (Supplemental Table 2). Therefore, NRAMP2 is a protein of the endosomal
179 network predominantly located in the TGN.

180

181 **Characterization of the role of NRAMP2 in Mn transport by heterologous expression** 182 **analysis in yeast**

183 To obtain insight into the Mn transport activity of NRAMP2, we tested its ability to
184 functionally complement yeast mutants inactivated in various Mn transport systems (Figure
185 5). The yeast NRAMP homolog Smf1p, which mediates Mn uptake at the plasma membrane
186 (Supek et al., 1996), was investigated first. Growth of the *smf1Δ* mutant, which is reduced in
187 the presence of EGTA due to Mn limitation, was not restored by the expression of
188 Arabidopsis *NRAMP2* (Figure 5A), unlike what was observed with Arabidopsis *NRAMP1*
189 (Curie et al., 2000; Thomine et al., 2000). We also previously showed that unlike NRAMP1,
190 NRAMP2 did not complement the plasma membrane iron uptake defect of the *fet3Δfet4Δ*
191 mutant (Curie et al., 2000). Therefore, NRAMP2 is unlikely to perform uptake at the plasma
192 membrane, a result that is consistent with our finding that NRAMP2 is located in an
193 intracellular compartment and that Mn acquisition is not affected in the *nramp2* mutant. Since
194 Smf2p in yeast had been described as an endomembrane Mn transporter (Cohen et al., 2000),
195 we tested whether NRAMP2 could functionally replace Smf2p. Growth of *smf2Δ*, which like
196 *smf1Δ* is reduced in the presence of EGTA, was fully restored by the expression of *NRAMP2*
197 (Figure 5A). Phenotypes of *smf2Δ* also include a strong decrease in cellular Mn content and
198 Mn SOD activity (Luk and Culotta, 2001). As expected, NRAMP2 restored both the Mn
199 content and Mn SOD activity of *smf2Δ* (Figure 5B,C), suggesting that NRAMP2 is a true
200 ortholog of the yeast Smf2p intracellular Mn transporter.

201 We also tested the capacity of NRAMP2 to rescue *pmr1Δ*, a yeast mutant lacking the
202 Mn transport ATPase for the Golgi. *pmr1Δ* is hypersensitive to high Mn due to increased Mn
203 accumulation in the cytosol. The expression of *NRAMP2* did not rescue the *pmr1Δ* phenotype
204 (Figure 5E). This finding suggests that NRAMP2 activity does not reduce cytosolic Mn

205 concentrations, which in turn implies that it mediates Mn import into the cytosol.
206 Interestingly, we found that NRAMP2 also efficiently rescued the sensitivity of *mtm1Δ* to
207 EGTA (Figure 5D). *mtm1Δ* was shown to misincorporate Fe instead of Mn into mitochondrial
208 SOD and can be rescued by supplying excess Mn to the cell (Yang et al., 2006; Whittaker et
209 al., 2015). Since NRAMP2 is a protein in the TGN membrane, its ability to rescue *mtm1Δ*
210 supports a role for this protein in improving cellular Mn availability.

211

212 **PSII activity is reduced in the *nramp2-3* mutant exposed to Mn starvation**

213 Since a cluster of four Mn atoms is associated with the oxygen-evolving complex of PSII, we
214 searched for defects of photosynthesis activity in the *nramp2-3* mutant that could explain its
215 slow growth under Mn-deficiency. We measured a number of photosynthesis parameters,
216 including maximal photochemical efficiency of PSII (Fv/Fm) and PSII operating efficiency
217 (Φ_{PSII}). The Fv/Fm values (close to 0.8) were unchanged for all genotypes grown under
218 control conditions (Figure 6, left panel). Under Mn limitation, the Fv/Fm value decreased by
219 30% in wild-type plants, thereby highlighting the requirement of Mn for PSII activity, and
220 noticeably dropped by an additional 10% in leaves of the *nramp2-3* (Figure, 6 right panel,
221 Supplemental Table 3) and *nramp2-4* mutants (Supplemental Table 3). This phenotype was
222 rescued in the two OxNR2-complemented lines (Figure 6, right panel, Supplemental Table 3).
223 Thus, NRAMP2 is required to maintain optimal PSII activity in conditions of limited Mn
224 availability. Electron transfer flow downstream of PSII, which is estimated by the Φ_{PSII} value,
225 was also more dramatically reduced under Mn deficient conditions in the two *nramp2* mutants
226 compared to wild-type plants and was restored to a higher value than wild type in the OxNR2
227 complemented lines (Supplemental Table 3). Therefore, photosynthesis efficiency under Mn
228 deficient conditions requires an active NRAMP2.

229

230 **The growth defect of the *nramp2* mutant is associated with reduced Mn levels in** 231 **chloroplasts and vacuoles**

232 To refine the role of NRAMP2 in the mobilization of internal Mn pools, Mn content was
233 measured in protoplasts and subcellular fractions of wild type, *nramp2-3* and the OxNR2 #3
234 complemented line grown in either Mn-replete or Mn-deficient conditions (Figure 7 and
235 Supplemental Table 4). In Mn-starved *nramp2-3* plants that display a strong phenotype, total
236 Mn content remained unchanged in protoplasts compared to protoplasts isolated from wild-
237 type plants (Figure 7A). This confirmed that inactivation of NRAMP2 affects the intracellular
238 distribution of Mn rather than total cellular content. We next tested whether the reduced

239 photosynthesis activity measured in *nramp2-3* was associated with a lower Mn content in the
240 chloroplasts. Under Mn deficiency, the Mn concentration dropped almost two-fold in the
241 chloroplasts of *nramp2-3* relative to wild-type plants, a defect that was rescued in the OxNR2
242 #3 line (Figure 7B). This suggested that reduced PSII activity in Mn-deficient *nramp2-3*
243 plants is caused by the lesser availability of Mn in the chloroplasts. Vacuoles were also
244 isolated from the same protoplasts in order to test for a general defect of Mn content in
245 organelles. Indeed, *nramp2-3* vacuoles showed reduced Mn concentration (Figure 7C),
246 confirming that NRAMP2 is required to maintain optimal Mn concentration in several
247 organelles. We therefore concluded that under Mn deficiency, NRAMP2 contributes to
248 building up an available pool of cellular Mn to be used by downstream compartments
249 including - but most likely not restricted to- chloroplasts and vacuoles.

250

251 **Cellular redox homeostasis is disturbed in the *nramp2* mutant**

252 The second prime target of Mn deficiency in plants is the mitochondrial superoxide
253 dismutase, or Mn SOD, the function of which is affected in the yeast *smf2Δ* mutant (Liu and
254 Culotta, 2001; this work). To test whether Mn SOD activity is affected in the *nramp2* mutant,
255 an in-gel SOD activity assay was performed (Figure 8). Despite the prolonged Mn starvation
256 treatment imposed in this experiment, Mn SOD activity remained unaffected regardless of the
257 genotype (Figure 8A). These data indicate that in contrast to PSII, Mn SOD activity is
258 maintained in the *nramp2* mutant under Mn deficient conditions. The most striking change
259 was observed for Cu/Zn SOD, the activity of which was strongly enhanced in *nramp2* plants
260 grown in Mn-limiting conditions (Figure 8A). Complementation of the mutant with NRAMP2
261 efficiently normalized the activity of Cu/Zn SOD (Figure 8A). A slight increase in Fe SOD
262 activity was also observed in Mn-deficient *nramp2-3* plants; contrary to Cu/Zn SOD,
263 however, Fe SOD activity was not rescued in the two OxNR2 complemented lines (Figure
264 8A).

265 The enhanced activity of Cu/Zn SOD revealed an imbalance of the redox status in Mn-
266 deficient *nramp2* cells. We thus monitored the production of reactive oxygen species (ROS)
267 in the *nramp2* mutant, especially the superoxide anion ($O_2^{\cdot-}$), which is the substrate of Cu/Zn
268 SOD. *In situ* detection of $O_2^{\cdot-}$ ions was carried out by staining mature leaves with nitroblue
269 tetrazolium (NBT). Leaves of the *nramp2-3* mutant showed strong purple NBT staining
270 regardless of the Mn regime, a phenotype that was mostly reverted in the OxNR2 #3
271 complemented line (Figure 8B). Increased NBT staining was not observed in the *nramp3*
272 *nramp4* double mutant (Figure 8B), even though this mutant shared several Mn-related

273 phenotypes with *nramp2* when exposed to Mn deficiency, including a growth defect and an
274 alteration of Mn homeostasis in chloroplasts (Lanquar et al., 2010).

275 In parallel, we tested whether NRAMP2 could rescue the oxidative stress of the *sod1Δ*
276 yeast mutant defective in cytosolic Cu/Zn SOD. *sod1Δ* showed sensitivity to as low as 1 mM
277 EGTA, a phenotype that was fully rescued by the expression of *NRAMP2* (Figure 8C). This
278 indicated that the pool of Mn displaced by NRAMP2 can efficiently replace cytosolic SOD
279 activity in yeast. Altogether, these results support the view that the Mn transport activity of
280 NRAMP2 takes part in the cellular antioxidant pathway.

281

282 **Leaf surface permeability is affected in the *nramp2-3* mutant**

283 Mn-starved *nramp2-3* plants displayed somewhat low turgor in leaves. A relationship
284 between tissue Mn content and cuticular wax synthesis in leaves has previously been pointed
285 out but is not well documented (Wilson et al., 1982; Hebborn et al., 2009). We therefore
286 investigated the permeability of the leaf surface in the *nramp2-3* mutant under Mn-replete or
287 deficient conditions (Figure 9). The integrity of the leaf cuticle can be revealed by staining
288 with an aqueous solution of the hydrophilic dye toluidine blue (TB) (Tanaka et al., 2004). TB-
289 exposed rosette leaves of the *nramp2-3* mutant showed an irregular punctuate staining after 10
290 minutes that contrasted with the intact cuticles of wild type and OxNR2 #3 leaves, suggesting
291 that the cuticles are permeable in *nramp2-3* leaves (Figure 9A). By contrast, the *nramp1-1*
292 mutant, whose Mn content is strongly reduced under Mn deficiency (Cailliatte et al., 2010),
293 showed the same intensity of TB staining as wild-type leaves (Supplemental Figure 4). This
294 suggested that, rather than Mn deficiency, it is the adequate allocation of Mn in cell
295 compartments that is crucial for producing leaf surface components. Finally, we measured the
296 cutin content in the leaves of *nramp2-3* and *NRAMP2*-complemented line OxNR2 #3 (Figure
297 9B, Supplemental File 1). Upon Mn deficiency, the cutin load was reduced by 40% in wild-
298 type plants, indicating that Mn is required for the production of an intact cuticle in
299 *Arabidopsis* leaves. Cutin content was unchanged in the *nramp2-3* mutant in control condition
300 but when exposed to Mn deficiency, *nramp2-3* was more severely affected than wild-type
301 plants, showing a more than 70% decrease. Consistent with TB staining, this phenotype of
302 *nramp2-3* in Mn-deficient conditions was rescued in the OxNR2 #3 complemented line.
303 Taken together, these results indicate that Mn compartmentalization by NRAMP2 plays an
304 important role in assembling the leaf cuticle in *Arabidopsis*.

305

306 Genetic interaction between NRAMP2 and the tonoplasmic NRAMP members NRAMP3
307 and NRAMP4

308 Hypersensitivity to Mn deficiency, reduced Mn content in chloroplasts and decreased
309 photosynthesis activity are features that are reminiscent of the phenotype of the *nramp3*
310 *nramp4* double mutant. We therefore tested functional redundancy between NRAMP2 on one
311 hand, and NRAMP3 and NRAMP4 on the other hand, by crossing the *nramp2* and *nramp3*
312 *nramp4* mutants. The triple *nramp2 nramp3 nramp4* mutant did not exhibit higher sensitivity
313 to Mn deficiency than the two parental lines, as shown by the equivalent reduction in
314 photosynthetic activity in all of these mutants (Supplemental Table 5). This suggested that the
315 three transporters act in the same pathway to provide Mn to the chloroplasts. Furthermore,
316 superoxide production was enhanced in the *nramp2 nramp3 nramp4* triple mutant, as
317 observed in *nramp2* (albeit seemingly less so) but not in *nramp3 nramp4*, thus indicating that
318 *NRAMP2* is epistatic to *NRAMP3/NRAMP4* (Supplemental Figure 5).

319

320

321 DISCUSSION

322 In this study, we characterized the phenotypic changes in Arabidopsis plants carrying a
323 knockdown allele of *NRAMP2*. *NRAMP2* is a protein localized in the TGN membrane that
324 can functionally replace the yeast endomembrane Mn transporter Smf2p. The *nramp2* mutant
325 displays pleiotropic defects that are exacerbated in Mn-deficient conditions and that
326 collectively point to a role of the *NRAMP2* transporter in the intracellular distribution of Mn
327 to its target compartments.

328

329 Mn is a physiological substrate for NRAMP2

330 Our study provides strong, although indirect, arguments in favor of *NRAMP2* acting as an Mn
331 transporter. The strongest argument is its ability to rescue the growth of a yeast mutant with
332 an inactivated *SMF2* gene, which encodes an NRAMP homolog with reported Mn transport
333 activity. *NRAMP2* can fully substitute for Smf2p, since its expression not only restored the
334 growth of the *smf2Δ* mutant in Mn-limiting conditions, but it also rescued its defective
335 MnSOD activity, suggesting that *NRAMP2* is a true ortholog of yeast Smf2p. In addition, we
336 obtained evidence that *NRAMP2* functions as a Mn transporter *in planta*. We found that
337 *NRAMP2* knockdown plants exhibited impaired growth, specifically in Mn-limiting
338 conditions, whereas *NRAMP2* overexpressing lines show hypertolerance to this treatment.
339 Furthermore, the Mn content in two cellular compartments, vacuoles and chloroplasts, was

340 markedly reduced in the *nramp2* mutant. Lastly, *NRAMP2* gene expression was induced in
341 response to Mn deficiency, which supports its involvement in Mn homeostasis. Thus, out of
342 the six NRAMP transporters in Arabidopsis, NRAMP2 represents the fourth member to play a
343 major role in Mn transport, next to NRAMP1, NRAMP3 and NRAMP4. The same
344 observation holds true for the characterized rice Os-NRAMP members and might be a general
345 feature of plant NRAMPs, thus distinguishing them from animal NRAMPs, which appear to
346 be more active in Fe transport.

347

348 **NRAMP2 is a resident TGN protein**

349 Unlike NRAMP1, NRAMP2 failed to rescue the plasma membrane Mn uptake of the yeast
350 $\Delta smf1$ mutant but successfully substituted for Mn transport by Smf2p, which is located on
351 vesicles of the yeast endomembrane system (Portnoy et al., 2000; Luk and Culotta, 2001). We
352 therefore made the assumption that NRAMP2 works intracellularly in the plant. In plant cells,
353 we found that NRAMP2 localized to a vesicular compartment. Using a set of endomembrane
354 markers, we showed that NRAMP2 primarily colocalized with the TGN marker SYP61. Since
355 endocytosed plasma membrane proteins are initially targeted to early endosomes (EE), and
356 since TGN can also function as an EE in plants (Uemura and Nakano, 2013), a possibility
357 existed that NRAMP2 was in fact cycling between the plasma membrane and TGN.
358 Interestingly, dual targeting of NRAMP1 between the plasma membrane and intracellular
359 vesicles of the endomembrane pathway was recently reported (Agorio et al., 2017). Unlike
360 NRAMP1, however, we did not find evidence for the presence of NRAMP2 at the cell
361 surface, regardless of whether NRAMP2-GFP-expressing plants were Mn-starved or treated
362 with the endocytosis inhibitor Tyrphostin A23. Consistent with our localization data,
363 NRAMP2, but none of the other Arabidopsis NRAMP isoforms, was identified in a proteomic
364 study performed on affinity purified SYP61-containing TGN vesicles (Drakakaki et al.,
365 2012). Therefore, NRAMP2 is likely a resident TGN protein.

366

367 **Loss of NRAMP2 affects Mn content in organelles**

368 Our data reveal that PSII activity is severely reduced in leaves of the *nramp2* mutant
369 exposed to Mn deficiency and that this decrease correlates with reduced Mn content in the
370 chloroplasts. This strongly suggests that NRAMP2 helps maintain chloroplastic Mn at an
371 optimal concentration for photosynthetic activity. We established that in addition to
372 chloroplast content, vacuolar Mn content is also significantly reduced in the *nramp2* mutant.
373 Thus, rather than specifically targeting the chloroplast, we suspected that NRAMP2 works

374 upstream of several organelles, probably by functioning at an early crossroad in the
375 distribution pathway. If this was indeed the case, we reasoned that NRAMP2 would likely
376 distribute Mn to most of its target organelles. Consistent with this idea, we found that
377 NRAMP2 complemented the defective growth of the mitochondrial mutant *mtm1*Δ under Mn
378 deficiency, suggesting that NRAMP2 increases Mn availability for this organelle. In
379 Arabidopsis, however, Mn SOD activity, which we used as a proxy for mitochondrial Mn
380 level, remained unchanged in the *nramp2* mutant, regardless of the Mn regime. This suggests
381 that Mn levels in mitochondria do not rely on the Mn transport activity of NRAMP2 or that an
382 alternative pathway exists that compensates for the absence of NRAMP2. Interestingly, Mn
383 SOD activity in wild-type plants was unaffected by Mn starvation, whereas the same
384 conditions efficiently depleted chloroplast content and affected PSII activity. A similar result
385 was previously reported (Lanquar et al., 2010). This suggests the existence of a hierarchy of
386 Mn allocation to the organelles in which maintaining mitochondrial Mn homeostasis is a
387 priority for the plant. Exactly the opposite result was obtained in *Chlamydomonas reinhardtii*,
388 where loss of activity of Mn SOD precedes the loss of PSII activity (Allen et al., 2007). In
389 conclusion, such a strong mechanism of preservation of Mn SOD activity in Mn-starved
390 Arabidopsis plants likely masks a potential impact of NRAMP2 mutation on mitochondrial
391 Mn content.

392 The chloroplastic pool of Mn was previously proposed to originate from the vacuole
393 because mutating the tonoplasmic Mn transporters NRAMP3 and NRAMP4, which remobilize
394 stored Mn from the vacuoles, led to a decreased concentration of Mn in chloroplasts (Lanquar
395 et al., 2010). The finding that metal content in chloroplasts is tightly linked to the capacity of
396 metal release from the vacuole was further demonstrated in two independent studies. When
397 both the Arabidopsis YSL4 and YSL6 chloroplast transporters were inactivated, which led to
398 increased Fe accumulation in the chloroplasts, the expression of *NRAMP3* and *NRAMP4* was
399 dramatically inhibited, presumably as a feed-back mechanism aimed at preventing Fe
400 overload into the chloroplasts (Divol et al., 2013). Furthermore, the steady state level of
401 ferritins, the stability of which depends on the presence of iron in the chloroplast, is
402 drastically reduced in the *nramp3 nramp4* double mutant background (Ravet et al., 2009).
403 Again, these results suggest that a direct link exists between Fe efflux from the vacuole and
404 Fe content in the chloroplasts. Altogether, these studies indicate that at least a large portion of
405 these metals contained in the chloroplasts originates from the vacuoles. Within the pathway
406 that provides Mn to the chloroplasts, several lines of evidence support the idea that the three
407 transporters, NRAMP2, NRAMP3 and NRAMP4, act together, with NRAMP2 operating

408 before the other two: i) The phenotype of hypersensitivity to Mn deficiency of the *nramp2*
409 *nramp3 nramp4* triple mutant is similar in intensity to that of the *nramp2* single mutant; ii)
410 The pleiotropic phenotypes of *nramp2* include all of the alterations of *nramp3 nramp4* but
411 also additional ones such as oxidative stress imbalance, vacuolar Mn depletion and cuticular
412 wax defects; and iii) *NRAMP2*, *NRAMP3* and *NRAMP4* have overlapping spatial expression
413 patterns and respond similarly to Mn deficiency. Together, these experiments argue against
414 the direct uptake of Mn from the cytosol and rather favor a strategy by which Mn first
415 accumulates into the vacuole prior to being dispatched to its target organelles. Favoring safe
416 metal storage into the vacuole, from which at least the chloroplast draws part of its supply,
417 may be a strategy used by the plant to prevent toxicity of these reactive metals in the cytosol.
418

419 **Mn and leaf surface permeability**

420 We demonstrated that leaf surface permeability and cutin production are disturbed specifically
421 in *nramp2-3* plants exposed to Mn deficiency and more generally as a result of Mn starvation.
422 A reduction in the epicuticular layer in response to Mn deficiency was previously described in
423 barley, where it was shown to be associated with a change in transpiration rate and water use
424 efficiency (Hebberner et al., 2009). This transformation, which may partly explain the reported
425 susceptibility of Mn-deficient crops to pathogens, might correspond to an adaptation of the
426 plant to reduced PSII activity. Furthermore, Mn availability was also found to regulate root
427 suberization, resulting in higher permeability of the stele in response to metal shortage
428 (Barberon et al., 2016). Interestingly, whereas both *nramp1* and *nramp2* are Mn-starved under
429 conditions of low Mn supply (Cailliatte et al., 2010), only the leaf permeability of *nramp2*
430 was more affected than wild-type plants in these experiments. Thus, it appears as though this
431 phenotype is caused by Mn deficiency in a specific cell compartment rather than by global
432 plant Mn status. Cuticle components are synthesized predominantly in the endoplasmic
433 reticulum (Yeats and Rose, 2013) and are then thought to be secreted to the cell wall via an
434 ER-Golgi route (Hoffmann-Benning and Kende, 1994). To date, no Mn-dependent enzymatic
435 activity has been identified in the biosynthetic pathway of cuticular components. As is the
436 case for the vacuole, chloroplast and mitochondria, the availability of Mn to endosomal
437 compartments such as the ER and Golgi apparatus might be reduced in the *nramp2* mutant,
438 hence affecting a potential Mn-containing enzyme involved in cuticle biosynthesis. It is
439 noteworthy that an important class of Mn-containing proteins of the cell is constituted by the
440 large family of glycosyl transferases (GT), which are mainly located in the Golgi, where they
441 glycosylate various substrates, among which are important glycoproteins of the cell wall.

442 Whether NRAMP2 brings Mn to Golgi-localized GTs or ER-localized cuticle biosynthetic
443 enzymes deserves further investigation.

444

445 **Oxidative stress level is elevated in *nramp2***

446 The *nramp2* mutant experiences redox imbalance under Mn-deficient conditions based on
447 increased Cu/Zn SOD activity and enhanced O_2^- production. The high O_2^- level in the mutant
448 is likely not provoked by reduced mitochondrial Mn SOD activity, as we found no
449 modification of this activity in *nramp2*, thus ruling out mitochondria as a source of O_2^- . Since
450 we measured increased Cu/Zn SOD, we speculated that O_2^- radicals produced by *nramp2*
451 originate from defective photosynthesis. Yet, the *nramp3 nramp4* double mutant, which also
452 displays reduced Mn content in chloroplasts and impaired Fv/Fm activity (Lanquar et al.,
453 2010), shows no defect in redox homeostasis. Therefore, the observation that only *nramp2*
454 plants showed higher oxidative stress levels strongly suggests that the localization of
455 NRAMP2 in the TGN, and therefore intracellular management of Mn pools, is central to the
456 cellular redox imbalance of the mutant.

457 In yeast, small molecular weight Mn complexes in the cytosol display SOD activity,
458 thereby acting as an alternative, parallel system to enzymatic SODs and providing an
459 explanation for the rescue of *sod1Δ* by Smf2p (McNaughton et al., 2010). We found in this
460 work that Arabidopsis NRAMP2 too can compensate for the absence of Sod1p in yeast. The
461 role of Mn-Pi or Mn^{2+} complexes with small organic molecules as potent scavengers of
462 superoxide has also been revealed in bacteria, and evidence that such antioxidant Mn species
463 exist in multicellular organisms was recently obtained in *Caenorhabditis elegans* and animal
464 sperm (Lin et al., 2006); reviewed in (Culotta and Daly, 2013). Thus, an appealing hypothesis,
465 which deserves future investigations, is that like its yeast ortholog, NRAMP2 could build up a
466 pool of cytosolic antioxidant Mn in Arabidopsis.

467

468 **NRAMP2 is crucial for Mn nutrition upon Mn limitation**

469 Within the cell, the TGN is a sorting hub for post-Golgi trafficking pathways involved in
470 secretory or vacuolar transport. The presence of NRAMP2 in the TGN suggests it plays a role
471 in the mobilization of Mn from, or into, these vesicles. Since proteins of the NRAMP family
472 use the proton gradient as a driving force (Nevo and Nelson, 2006), they are known to
473 transport metals from a more acidic to a less acidic compartment. Consequently, except for
474 the few studies that proposed that transport by NRAMP occurs in the direction of the exit of
475 metals from the cytosol (Techau et al., 2007),(Garcia-Rodriguez et al., 2015), the vast

476 majority of the reported NRAMP transporters, including all plant members, import metals
477 into the cytosol (Cailliatte et al., 2010). Following the proton cotransport dogma, the presence
478 of NRAMP2 on TGN vesicles, which are more acidic than the cytosol (Martiniere et al.,
479 2013), is consistent with NRAMP2 mediating Mn influx into the cytosol. In addition, the
480 failure of NRAMP2 to rescue the *pmr1Δ* yeast mutant defective in Golgi Mn uptake also
481 argues against an activity of NRAMP2 in transport toward the TGN lumen. Several
482 observations support the hypothesis that NRAMP2 releases Mn from the TGN into the
483 cytosol and hence contributes to the build up of a cytosolic Mn pool that would be used to
484 feed Mn both to downstream organelles and to the anti-oxidant machinery of the cell: i) the
485 Mn content in two organelles, vacuoles and chloroplasts, correlates with the expression level
486 of NRAMP2: vacuoles and chloroplasts of the *nramp2* mutant both harbor low Mn content; ii)
487 in yeast, NRAMP2 expression rescues the mitochondrial *mtm1Δ* mutant, the growth of which
488 depends on high Mn supply to the mitochondria (Yang et al., 2006); these two arguments
489 strongly support a role for NRAMP2 in fueling the cytosolic Mn pool, which serves as a
490 source of Mn to the main organelles; iii) NRAMP2 is also able to functionally compensate for
491 the absence of cytosolic Sod1p in yeast, which we propose may occur through the
492 accumulation of cytosolic Mn antioxidant species having SOD activity. If a similar alternate
493 SOD system relying on Mn antioxidant species in the cytosol exists in plants, NRAMP2
494 represents a reasonable candidate to supply these from vesicular compartments.

495 Based on the phenotypes of an *nramp2* knockdown allele and its combination with the
496 *nramp3* and *nramp4* mutations, we propose a model in which under Mn-limiting conditions, a
497 pool of Mn stored in the TGN is released by NRAMP2 and carried by a yet-to-be identified
498 pathway to the vacuole, from which it is secreted by NRAMP3 and NRAMP4 to provide a
499 significant portion of the Mn ions that reach the chloroplasts (Figure 10). In-depth analysis of
500 the cellular function of candidate Mn transporters, including members of the ECA, MTP and
501 NRAMP families, should identify additional important actors and shed further light into the
502 Mn trafficking pathway in plant cells, although chemical or genetically-encoded Mn sensors
503 will be needed to image Mn movement between cell compartments.

504

505

506 **METHODS**

507

508 **Plant materials and growth conditions**

509 Two *Arabidopsis thaliana* *NRAMP2* mutant lines were used: *nramp2-3* (unreferenced SALK
510 line kindly provided by Dr. Jose Alonso) and *nramp2-4* (GK-306A04), both containing a T-
511 DNA inserted in the 5'-UTR of the *NRAMP2* gene, at 68 base pairs and 43 base pairs
512 upstream of the ATG start codon, respectively. The *nramp1-1* mutant was described
513 previously (Cailliatte et al., 2010). The *nramp3-2 nramp4-2* double mutant was generated by
514 crossing SALK line 023049 (*nramp3-2*) with SALK line 003737 (*nramp4-2*).

515 *Arabidopsis* seedlings (ecotype Columbia-0) were grown *in vitro* under sterile conditions
516 at 21°C with an 8h-light (composed of 50% sodium-vapor lamps and 50% metal halide (HQI)
517 lamps)/16h-dark cycle. Seeds were surface sterilized and sown on half-strength Murashige
518 and Skoog medium containing 1% sucrose, 2.5 mM MES and either 0.6% agar for horizontal
519 cultures or 1% agar for vertical cultures. The pH was adjusted to 5.7 with KOH.

520 For the hydroponic growth experiments, seeds were sown on vertical plates. 8-day-old
521 seedlings were placed in a modified Hoagland solution containing 0.25 mM NH_4NO_3 , 1 mM
522 $\text{Ca}(\text{NO}_3)_2$, 0.2 mM KH_2PO_4 , 1.4 mM KNO_3 , 0.4 mM MgSO_4 , 20 μM Fe(III)-Na-EDTA, 4.5
523 μM H_3BO_3 , 0.03 μM CuSO_4 , 0.07 μM ZnSO_4 , and 0.02 mM MoO_3 . For control conditions,
524 the medium was supplemented with 5 μM MnSO_4 . The nutrient solution was renewed
525 weekly. The hydroponic cultures were grown in a controlled environment (8h-light 23°C/16h-
526 dark cycles, 20°C, 200 $\mu\text{E}\cdot\text{s}^{-1}$ light intensity, 70% relative humidity) for the amount of time
527 indicated in the figure legends.

528

529 **Plasmid constructs**

530 For tissue-specific expression studies, 983 bp of the promoter region located upstream of the
531 *NRAMP2* initiation codon were amplified by PCR from BAC F8G22 using forward primers
532 OCC53 and OCC54 (see list of primers in Supplemental Table 6), introducing an *XbaI* and
533 *NcoI* site, respectively. The PCR product was cloned into the pBKS⁺-GUS vector. The
534 *ProNRAMP2:GUS* fusion cassette was then transferred into the *XbaI* site of the pGreen29
535 binary vector. For the *ProUBI0:NRAMP2-GFP* fusion construct, the *NRAMP2* cDNA was
536 amplified without its stop codon using primers NR2_ORF-F and NR2_ORF-R and cloned
537 into the pDONR 207 entry vector (Gateway, Invitrogen). The *NRAMP2* ORF was then
538 subcloned into the pUBC-GFP-Dest vector (Grefen et al., 2010) to generate a C-terminal GFP
539 fusion. The GV3101 strain of *Agrobacterium tumefaciens* containing the *ProNRAMP2:GUS*
540 and *ProUBI0:NRAMP2-GFP* constructs were transformed into *Arabidopsis* ecotype Col-0
541 wild-type and *nramp2-3*, respectively, by the floral dip method (Clough and Bent, 1998).

542

543 **Cell fractionation**

544 **Chloroplasts isolation.** Protoplasts were isolated by enzymatic digestion of approximately 3
545 g of leaves cut in 1-2 mm-wide stripes in 10 mL of MCP buffer (500 mM sorbitol, 1 mM
546 CaCl_2 , and 20 mM MES, adjusted to pH 6 with KOH) supplemented with 0.4% (w/v)
547 Macerozyme R10 (Duchefa Biochemie) and 0.8% (w/v) Cellulase Onozuka R10 (Duchefa
548 Biochemie) at 30°C for 1 h 30 min. The protoplasts were filtered through a 75- μm nylon
549 mesh, pelleted (200g, 5 min, 4°C), and washed twice with MCP buffer. The protoplasts were
550 diluted to 2×10^6 cells mL^{-1} and lysed by filtration through a polyester mesh (Spectrum, pore
551 size 21 μm). The lysed protoplasts were kept on ice. Percoll step gradient: bottom phase, 1
552 volume of 85% Percoll in washing medium (300 mM sorbitol, 40 mM Tricine pH 7.6, 2.5
553 mM EDTA, and 0.5 mM MgCl_2); Top phase, 1 volume of 40% Percoll in washing medium.
554 Chloroplasts were isolated by loading the protoplast lysate on top of the Percoll step gradient
555 followed by centrifugation (2500g, 10 min, 4°C, without brake) in a swinging rotor. Intact
556 chloroplasts were recovered by centrifugation at 200 g for 5 min at 4°C (with no brake) from
557 the 40/85% Percoll interphase and washed two times with cold washing medium . The
558 integrity of the chloroplasts was verified by microscopy, and the number of chloroplasts was
559 estimated by counting with a Neubauer chamber.

560 **Vacuole isolation.** The vacuole isolation was carried out as previously described (Lanquar et
561 at., 2010) with some modifications. Briefly, the protoplasts were lysed by the addition of an
562 equal volume of protoplast lysis buffer (200 mM sorbitol, 10% [w/v] Ficoll 400, 20 mM
563 EDTA, 10 mM HEPES-KOH, pH 8, 0.15% [w/v] bovine serum albumin, and 2 mM
564 dithiothreitol [DTT] and 5 $\mu\text{g}/\text{ml}$ neutral red) pre-warmed at 37°C. Protoplast lysis was
565 monitored microscopically, and lysed protoplasts were kept on ice. Vacuoles were isolated
566 using a step gradient in swinging rotors (1,500g, 20 min, 4°C): bottom phase: 1 volume of
567 lysed protoplasts; middle phase: 0.8 volume of lysis buffer diluted in vacuole buffer to a final
568 concentration of 4% (w/v) Ficoll; top phase: 0.2 volume of vacuole buffer (500 mM sorbitol,
569 10 mM HEPES pH 7.5 [KOH], 0.15% [w/v] bovine serum albumin and 4 mM DTT).
570 Vacuoles were recovered as a thin red layer at the interface between the middle phase and the
571 top phase. The purity of the vacuole preparation was monitored by microscopy and the
572 number of vacuoles was estimated by counting with a Neubauer chamber.

573

574 **Gene expression analysis**

575 Total RNA was extracted using the TRIZOL reagent (Invitrogen) following the
576 manufacturer's instructions. Reverse transcription was performed with oligo d(T) primers on

577 1 to 2 µg of total RNA digested with DNase I (Thermo Scientific) using a RevertAid First
578 Strand cDNA Synthesis Kit (Thermo Scientific) according to the manufacturer's protocols.
579 The qPCRs were performed on the Roche Light Cycler 480 II instrument using the primer sets
580 listed in Supplemental Table 6 and SYBR[®] Premix Ex Taq (Tli RNaseH Plus), Bulk (Takara).
581

582 **GUS histochemical analysis**

583 Samples were vacuum infiltrated for 20 min and incubated for 18h in GUS buffer containing
584 50 mM NaPO₄ pH 7.4, 2 mM ferrocyanide, 2 mM ferricyanide, 0.05% Triton X-100, and 1
585 mM X-Gluc (5-bromo-4-chloro-3-indolyl-β-D-glucuronide). The samples were then soaked in
586 phosphate buffer (50 mM NaPO₄ pH 7.2) and prefixed for 3 h in phosphate buffer containing
587 2% paraformaldehyde and 0.5% glutaraldehyde. The samples were cleared with successive
588 washes of increasing ethanol concentrations from 50 to 100% for direct observation or
589 embedded in 2-hydroxyethyl methacrylate (Technovit 7100; Heraeus-Kulzer). Thin cross-
590 sections (5 µm) were cut using a Leica RM 2165 microtome, counter-stained with Schiff dye,
591 and observed under an Olympus BH2 microscope.

592

593 **Yeast strains and growth conditions**

594 Yeast cells were grown at 30°C in YPD medium (2% glucose, 2% tryptone and 1% yeast
595 extract) or SD medium (2% glucose, 0.7% yeast nitrogen base with ammonium sulfate and 50
596 mM succinic acid pH5.5). Wild-type BY4741 (*MATa; his3, leu2, met15, ura3*); *smf1Δ*
597 (*MATa; his3, leu2, met15, ura3, smf1::kanMX4*), *smf2Δ* (*MATa; his3, leu2, met15, ura3,*
598 *smf2::kanMX4*), *mtm1Δ* (*MATa; his3, leu2, met15, ura3, mtm1::kanMX4*), *pmr1Δ* (*MATa;*
599 *his3, leu2, met15, ura3, pmr1::kanMX4*) and *sod1Δ*
600 (*MATa his3 ::1 leu2::0 met15::0 ura3::0 sod1::kanMX4*) cells were transformed with
601 pYPGE15-*NRAMP2* (Curie et al., 2000), where *NRAMP2* is expressed under the control of
602 the constitutive high yeast phospho-glycerate kinase (PGK) promoter, or pYPGE15 empty
603 vector using electroporation. Yeast transformants were selected on medium lacking uracil.
604 For growth tests, yeast cells were first grown in liquid culture overnight at 30°C in SD 605
606 medium. The cultures were adjusted to OD₆₀₀ = 0.3 and aliquots of 5-fold serial dilutions were
607 plated on 2% (w/v) agar plates containing SD-Ura medium supplemented with EGTA
608 or MnSO₄. In the case of EGTA plates, SD medium was prepared with 0.7% YNB with low
609 metal concentration (US Biological, USA). To monitor the steady-state manganese levels
610 in yeast cells, the strains were grown in 20 ml SD-Ura medium to an OD₆₀₀ = 1.5, pelleted and
washed three times with 10 mM EDTA and twice with deionized water.

611

612 **Superoxide dismutase activity**

613 **In yeast:** Yeast cells were propagated in YPD medium to an OD₆₀₀ of 1.5, harvested and
614 washed with cold water before being broken by agitation in the presence of glass-beads in
615 extraction buffer (100 mM NaPO₄ pH 7.8, 50 mM NaCl, 5 mM EDTA, 5 mM EGTA, 0.1%
616 Triton X-100, 100 µg/ml phenylmethylsulfonyl fluoride, 1 µg/ml pepstatin A and 1 µg/ml
617 leupeptin). The homogenate was centrifuged for 5 min at 2500g and the protein pellet was
618 solubilized in extraction buffer.

619 **In plants:** Leaves were ground in liquid nitrogen and resuspended in cold extraction buffer
620 (40 mM K₂HPO₄, 10 mM KH₂PO₄, 6 mM ascorbic acid, 0.05% β-mercaptoethanol and 0.2%
621 Triton X-100) for 2 min, followed by 10 min centrifugation at 14,000 rpm at 4°C.

622 Proteins were loaded onto a 12% non-denaturing PAGE gel and the SOD activity was
623 measured by nitroblue tetrazolium (NBT) staining. Briefly, the gel was soaked in NBT
624 solution (1 mg/ml) for 20 min in the dark and transferred into staining solution (33 mM
625 K₂HPO₄, 3.3 mM KH₂PO₄, 1 mg/ml riboflavin and 0.3% TEMED) for 20 min in the dark.
626 The gel was rinsed in distilled water before being exposed to high light until the bands
627 appeared.

628

629 **Manganese content measurements**

630 The roots were washed for 10 min with 10 mM EDTA and 5 min with 30 mM MgCl₂,
631 followed by two rinses in deionized water. Shoots were simply rinsed twice with deionized
632 water. Plant samples and yeast pellets were dried at 80°C for 4 days. For mineralization, the
633 tissues were digested completely in 50% HNO₃ and 7.5% H₂O₂ using the Speedwave 2
634 microwave digestion system (Berghof, Germany). Mn measurements were performed by
635 atomic emission spectrometry (4200 MP-AES, Agilent).

636

637 **Photosynthesis fluorescence measurements**

638 A kinetic imaging fluorometer (FluorCam FC 800-O, Photon Systems Instruments, Czech
639 Republic) was used to capture fluorescence images and to estimate the maximal
640 photochemical efficiency of PSII [$F_v/F_m = (F_m - F_o)/F_m$] and effective photochemical
641 efficiency of PSII (Φ_{PSII}) parameters. Control and Mn-free Arabidopsis plants were dark-
642 adapted (30 min), and all fluorescence measurements were performed *in vivo* at room
643 temperature. Saturating flashes ($1000 \mu\text{mol} \cdot \text{m}^{-2} \cdot \text{s}^{-1}$) were used to measure the maximum
644 fluorescence.

645

646 **Chlorophyll measurements**

647 A SPAD meter (SPAD-502Plus, Konica-Minolta, Japan) was used to take SPAD values from
648 two fully expanded young leaves on each plant. A total of six plants were measured for each
649 genotype and growth condition, and three SPAD values per leaf were averaged as the mean
650 SPAD value of the leaf.

651

652 **Detection of superoxide radicals**

653 O_2^- ions were visualized by staining leaves (leaf # 8-10) with nitroblue tetrazolium (NBT).
654 Briefly, excised leaves were vacuum infiltrated in NBT staining solution (1 mg/ml NBT, 10
655 mM Na_2HPO_4) for 20 min and incubated for 2-3 hours under the light. Chlorophyll was
656 removed by incubating the leaves for 5 min in boiling 96% ethanol. After cooling, the leaves
657 were immersed in water and photographed in 10% glycerol.

658

659 **Permeability test with toluidine blue**

660 Excised leaves were submerged into an aqueous solution of filtered 0.05% (w/v) TB in a
661 small Petri dish for the indicated amount of time. The leaves were gently washed with water
662 to remove excess TB.

663

664 **Cutin load analysis**

665 Three to five fully developed leaves were used per replicate. Freshly collected leaves were
666 scanned to measure their surfaces and immediately incubated in hot isopropanol for 30 min at
667 85°C. After cooling, the solvent was eliminated and the leaves were extensively delipidated
668 by extracting the soluble lipids successively with $CHCl_3:CH_3OH$ (2:1, v/v), $CHCl_3:CH_3OH$
669 (1:1, v/v), $CHCl_3:CH_3OH$ (1:2, v/v), and CH_3OH . Each delipidation step was performed for
670 24 h at room temperature on a rotating wheel at 40 rpm. The delipidated leaves were dried in
671 a fume hood at room temperature for 2 days and then in a desiccator for another 2 days. Cutin
672 analysis was then performed as described previously (Domergue et al., 2010).

673

674 **Confocal microscopy analysis**

675 *Nicotiana tabacum* leaves were agro-infiltrated with the recombinant *Agrobacterium*
676 *tumefaciens* strains (strain GV3101, infiltration solution $OD_{600} = 0.1$). After two days,
677 confocal imaging was performed using a Leica TCS SP8 laser scanning microscope with a

678 63X oil N.A. 1.4 immersion objective. Emission fluorescence of CFP, GFP and mCherry was
679 collected in line sequential scanning mode at 458 nm, 488 nm and 561 nm excitation,
680 respectively. The emitted signal was collected between 462-485 nm, 500-535 and 580-630 for
681 CFP, GFP and mCherry/RFP, respectively, and images were acquired with the best lateral and
682 axial resolution (pixel size 60/70 nm). Images were processed using ImageJ software. For the
683 FM4-64 endocytosis experiments, roots of 7-day-old Arabidopsis seedlings were incubated
684 for 5 min in 10 μ M FM4-64 and rinsed with water at the time indicated in the figure legends.
685 The set of cell compartment markers (plasmids or Arabidopsis lines) used was as follows: Px-
686 rk983-mCherry (Nelson et al., 2002), Arabidopsis Wave lines (Geldner et al., 2009), ERD2-
687 CFP (Brandizzi et al., 2002), and SYP61-mRFP (Foresti et al., 2010).

688 Colocalization coefficients were computed with the JACoP plugin (r_{pearson} , Pearson
689 correlation coefficient; M1 and M2, Mander's overlap coefficients above threshold) (Bolte
690 and Cordelieres, 2006). In each experiment, 7 to 10 cells from the root elongation zone were
691 analyzed individually for each genotype.

692

693 **Accession numbers**

694 Sequence data from this article can be found in the Arabidopsis Genome Initiative or
695 GenBank/EMBL databases under accession numbers At1g80830 (NRAMP1), At1g47240
696 (NRAMP2), At2g23150 (NRAMP3), At5g67330 (NRAMP4), and At3g18780 (ACT2).

697

698 **Supplemental Data**

699 **Supplemental Figure 1.** *nramp2* mutant alleles are chlorotic under Mn deficiency.

700 **Supplemental Figure 2.** Expression of *NRAMP1* is not modified in the *nramp2-3* mutant.

701 **Supplemental Figure 3.** Confocal microscopy observations of NRAMP2-GFP fluorescence
702 and colocalization with markers of various cell compartments.

703 **Supplemental Figure 4.** *nramp2-3*, but not the Mn-deficient mutant *nramp1-1*, shows leaf
704 permeability defects.

705 **Supplemental Figure 5.** Production of superoxide ions in the *nramp2 nramp3 nramp4* triple
706 mutant.

707 **Supplemental Table 1.** Mn concentration ($\mu\text{g}\cdot\text{g}^{-1}$ DW) in rosette leaves and roots of WT,
708 *nramp2-3* and the *OxNR2 #3* and *OxNR2 #6* complemented lines.

709 **Supplemental Table 2.** Quantitative analysis of NRAMP2-GFP colocalization with Golgi
710 markers.

711 **Supplemental Table 3.** Photosynthetic activity of *nramp2* mutant alleles and the
712 complemented line OxNR2 #3.
713 **Supplemental Table 4.** Mn content is altered in vacuoles and chloroplasts of the *nramp2-3*
714 mutant.
715 **Supplemental Table 5.** Photosynthetic activity of single *nramp2-3*, double *nramp3-2*
716 *nramp4-2* and triple *nramp2-3 nramp3-2 nramp4-2* mutants.
717 **Supplemental Table 6.** List of the gene-specific primers used.
718 **Supplemental File 1.** ANOVA Table.

719
720

721 **ACKNOWLEDGEMENTS**

722 This work was funded by the Agence Nationale pour la Recherche through the ANR grants
723 PLANTMAN (ANR-2011-BSV6-004) and MANOMICS (ANR-2011-ISV6-001-01), by the
724 Centre National de la Recherche Scientifique and by the Institut National de la Recherche
725 Agronomique. Microscopy observations were made at the Montpellier RIO Imaging facility
726 (<http://www.mri.cnrs.fr/>). We thank Dr. Jose Alonso for providing *nramp2-3* seeds. We are
727 indebted to Sandrine Chay and Brigitte Touraine for assistance with MP-AES and FluorCam
728 measurements, respectively. S.A.-M. and L.C. were supported by the Agence Nationale pour
729 la Recherche, and R.C. was supported by the French Ministry of Agriculture and Fisheries.

730

731 **AUTHOR CONTRIBUTIONS**

732 **S.A., R.C., S.M. and C.C. designed the research. S.A., R.C., C.A., L.D., D.C., L.C., F.D.**
733 **performed research and analyzed data. C.A. performed confocal imaging experiments**
734 **and statistical analysis of colocalizations. F.D. performed lipid analyses. J.F.B.**
735 **contributed to discussions and constructive comments on the manuscript. The**
736 **manuscript was written by S.A. and C.C.**

737

738 **NOTE ADDED IN PROOF**

739 While this manuscript was under revision, two mutant alleles of *NRAMP2* (*nramp2-1* and
740 *nramp2-2*) were reported [Gao, H., Xie, W., Yang, C., Xu, J., Li, J., Wang, H., Chen, X.,
741 and Huang, C.F. (2017) NRAMP2, a trans-Golgi network-localized manganese transporter,
742 is required for Arabidopsis root growth under manganese deficiency. New Phytologist doi:
743 10.1111/nph.14783].

744

745

746

747 FIGURES LEGENDS

748 **Figure 1.** *nramp2* mutants are hypersensitive to Mn deficiency.

749 **(A)** Position of the T-DNA insertion in two *nramp2* mutant alleles relative to the ATG start
750 codon.

751 **(B)** Relative *NRAMP2* transcript abundance measured by qRT-PCR in *nramp2* mutant alleles
752 and in the two *nramp2-3* complemented lines O_xNR2 #3 and O_xNR2 #6. Transcript levels are
753 expressed relative to those of the reference gene *ACTIN* ± SD (n=3 measurements per
754 sample). **(C)** Phenotypes of plants of the indicated genetic backgrounds grown for one week
755 in Mn-replete conditions (5 μM Mn SO₄) followed by 3 additional weeks in Mn-free
756 hydroponic conditions.

757 **(D)** and **(E)** Shoot **(D)** and root **(E)** biomass production of the plants presented in C (-Mn) or
758 in Mn replete conditions (Control). Data are from one representative experiment (n = 10
759 plants). Panels D and E share color code legends. Mean ± SD. Asterisks indicate values
760 significantly different from those of wild type (Student's *t* test, * P-value < 0.05, ** P-value <
761 0.01). Scale bars = 1 cm.

762

763 **Figure 2.** *nramp2-3* shows Mn homeostasis defects under Mn-free conditions.

764 **(A)** Mn content in the Mn-deficient plants presented in Figure 1 and in control plants grown
765 in parallel in Mn-replete conditions shown in Supplemental Figure 1D. Data are from one
766 representative experiment (n = 4 plants). DW: Dry weight. Mean ± SD. Asterisks indicate
767 values significantly different from those of wild type (Student's *t* test, * P-value < 0.01).

768

769 **Figure 3.** *NRAMP2* expression analysis.

770 **(A)** Relative *NRAMP2* transcript abundance in roots and shoots measured by qRT-PCR.
771 Transcript levels are expressed relative to those of the reference gene *ACTIN* ± SD (n=3
772 technical replicates). Wild-type plants were grown hydroponically for 3 weeks in control (5
773 μM MnSO₄) or in Mn-free (-Mn) conditions. Data are from one representative experiment (n
774 = 3 plants). Mean ± SD. Asterisks indicate values significantly different from those of control
775 conditions (Student's *t* test, * P-value < 0.01).

776 **(B)** Histochemical staining of GUS activity in *proNRAMP2:GUS*-transformed Arabidopsis
777 grown in Mn-replete conditions. **(a)** 6-day-old seedling. **(b)** Young rosette leaf. **(c)** Mature
778 rosette leaf. **(d)** Primary root of a one-week-old plant in the mature zone. **(e)** Root cross-

779 section in the mature zone. Ep: epidermis, Co: cortex, End: endodermis, Pe: pericycle. Data
780 are shown for one representative line out of 3 independent lines.

781

782 **Figure 4.** NRAMP2 is localized to the Trans-Golgi Network.

783 (A) and (B) Fluorescence pattern of the NRAMP2-GFP construct and kinetics of
784 colocalization with the endocytic tracer FM4-64 (A: 2 min, B: 15 min) observed by confocal
785 microscopy in roots of 5-day-old plants.

786 (C) and (D) Colocalization of NRAMP2-GFP with markers for cis-Golgi (ERD2-CFP), trans-
787 Golgi (ST-RFP), and TGN (SYP61-GFP) transiently co-expressed in tobacco leaves. Inserts
788 show a close-up image of the association of NRAMP2-GFP with the various Golgi
789 subcompartments. Scale bars: 5 μ m.

790 (E) and (F) pixel intensity profiles of GFP (green), RFP (magenta) and CFP (blue) were
791 measured along a line spanning the sub-compartments magnified in the close-up inserts
792 shown in (C) and (D), respectively.

793

794 **Figure 5.** NRAMP2 complements the *smf2* Δ and *mtm1* Δ yeast mutants.

795 (A), (D) and (E) Growth tests of wild type (BY4741) and mutant yeast strains *smf1* Δ (A),
796 *smf2* Δ (A,E), *mtm1* Δ (D) and *pmr1* Δ (E) transformed with the pYPGE15 empty vector (E.V.)
797 or the pYPGE15/NRAMP2 construct (NRAMP2). 5-fold serial dilutions were plated on SD-
798 Ura supplemented or not (control) with the amount of EGTA indicated in the figure panels
799 (A, D) or 2 mM MnSO₄ (E) and incubated at 30°C for 3 days.

800 (A) NRAMP2 restores *smf2* Δ mutant tolerance to Mn deficiency.

801 (B) Mn content measured by MP-AES in yeast strains grown in liquid SD -URA for 24 hours.
802 Mean \pm SD (n-3). Asterisks indicate values significantly different from those of wild type
803 (Student's *t* test, * P-value < 0.01).

804 (C) *In gel* SOD activity assay carried out on proteins extracted from yeast strains grown as in
805 (B).

806 (D) NRAMP2 restores *mtm1* Δ mutant tolerance to Mn deficiency.

807 (E) NRAMP2 fails to rescue *pmr1* Δ mutant sensitivity to excess Mn and does not reduce
808 wild-type or *smf2* Δ tolerance to excess Mn.

809

810 **Figure 6.** Photosynthetic activity is impaired in *nramp2-3*.

811 Maximum PSII efficiency (Fv/Fm) measured on rosette leaves of wild-type, *nramp2-3* and
812 two complemented lines grown for 4 weeks in hydroponic conditions in the presence of Mn

813 (+Mn) or 1 week with Mn and transferred to medium without Mn for 3 additional weeks (-
814 Mn). Mean \pm SD (n = 10 leaves from 10 plants). Asterisks indicate values significantly
815 different from those of wild type (Student's *t* test, * P-value < 0.05, ** P-value < 0.01).

816

817 **Figure 7.** Vacuoles and chloroplasts of the *nramp2-3* mutant contain less Mn than wild type.
818 (A) to (C) Mn content was measured on isolated protoplasts (A), chloroplasts (B) or vacuoles
819 (C) in wild-type, *nramp2-3* and the OxNR2 #3 complemented line grown in hydroponic
820 cultures for one week in the presence of Mn followed by three additional weeks in the
821 absence of Mn. All panels share color code legends. Metal concentration was determined by
822 MP-AES and is expressed as ng per 10⁶ protoplasts or organelles. Data are from one
823 representative experiment (n = 4 plants). Mean \pm SD. Asterisks indicate values significantly
824 different from those of wild type (Student's *t* test, * P-value < 0.01).

825

826 **Figure 8.** *nramp2-3* displays high levels of oxidative stress.

827 (A) and (B) Plants of the indicated genotypes were cultivated in hydroponic conditions for 4
828 weeks in the presence of Mn (+Mn) or 1 week with Mn and transferred to medium without
829 Mn for 3 additional weeks (-Mn). (A) In-gel SOD activity assay performed using total
830 proteins extracted from leaves. (B) Detection of superoxide ion production in Mn replete or
831 Mn-starved leaves by staining with nitroblue tetrazolium (NBT).
832 (C) NRAMP2 rescues the sensitivity of the yeast *sod1Δ* mutant to Mn deficiency. 5-fold serial
833 dilutions were plated on SD-Ura supplemented with 1 mM EGTA (right) or not (Control,
834 left). Arrows indicate the growth rescue of *smf2Δ* by NRAMP2.

835

836 **Figure 9.** *nramp2-3* shows cell wall permeability defects.

837 Plants of the indicated genotypes were grown in hydroponic conditions for 3 weeks in the
838 presence of Mn followed by an additional week in the presence (+ Mn) or absence of Mn (-
839 Mn).

840 (A) Permeability of the leaf surface was examined by staining entire leaves with Toluidine
841 blue for 10 min. Inserts show a closeup view of the TB-stained spots on the leaves.
842 (B) Cutin load per surface unit of leaf measured by GC-MS. Mean \pm SD (n= 4 leaves from 4
843 plants). Values that are not significantly different are noted with the same letter (ANOVA, α
844 risk 5%, Supplemental File 1).

845

846 **Figure 10.** Hypothetical model of the function of NRAMP2 in cellular Mn distribution.

847 When NRAMP2 is nearly absent (*nramp2* knockdown mutants), plants are hypersensitive to
848 Mn deficiency and PSII activity is markedly impaired. NRAMP2 is a transporter localized in
849 the TGN membrane, where it likely exports Mn from the TGN lumen to the cytosol. In doing
850 so, NRAMP2 builds up a pool of Mn (red circle) that, based on the pleiotropic effects of the
851 *NRAMP2* mutation, is used to feed an array of downstream organelles: vacuoles and
852 chloroplasts, since both display decreased Mn content in *nramp2-3*, and mitochondria based
853 on the ability of NRAMP2 to complement yeast *mtm1Δ*. Combining *nramp2-3* with *nramp3-2*
854 and *nramp4-2* mutations suggests that NRAMP2 and NRAMP3/NRAMP4 act in concert to
855 provide Mn to the PSII, NRAMP2 being epistatic to the other two.

856

857

858 REFERENCES

- 859 Agorio, A., Giraudat, J., Bianchi, M.W., Marion, J., Espagne, C.,
860 Castaings, L., Lelievre, F., Curie, C., Thomine, S., and Merlot, S.
861 (2017). Phosphatidylinositol 3-phosphate-binding protein AtPH1
862 controls the localization of the metal transporter NRAMP1 in
863 Arabidopsis. *Proc Natl Acad Sci U S A* **114**, E3354-E3363.
- 864 Allen, M.D., Kropat, J., Tottey, S., Del Campo, J.A., and Merchant, S.S.
865 (2007). Manganese deficiency in *Chlamydomonas* results in loss of
866 photosystem II and MnSOD function, sensitivity to peroxides, and
867 secondary phosphorus and iron deficiency. *Plant Physiol* **143**, 263-277.
- 868 Barberon, M., Vermeer, J.E., De Bellis, D., Wang, P., Naseer, S., Andersen,
869 T.G., Humbel, B.M., Nawrath, C., Takano, J., Salt, D.E., and Geldner,
870 N. (2016). Adaptation of root function by nutrient-induced plasticity
871 of endodermal differentiation. *Cell* **164**, 447-459.
- 872 Bolte, S., and Cordelieres, F.P. (2006). A guided tour into subcellular
873 colocalization analysis in light microscopy. *J Microsc* **224**, 213-232.
- 874 Brandizzi, F., Frangne, N., Marc-Martin, S., Hawes, C., Neuhaus, J.M., and
875 Paris, N. (2002). The destination for single-pass membrane proteins
876 is influenced markedly by the length of the hydrophobic domain. *Plant*
877 *Cell* **14**, 1077-1092.
- 878 Cailliatte, R., Lapeyre, B., Briat, J.F., Mari, S., and Curie, C. (2009).
879 The NRAMP6 metal transporter contributes to cadmium toxicity. *Biochem*
880 *J* **422**, 217-228.
- 881 Cailliatte, R., Schikora, A., Briat, J.F., Mari, S., and Curie, C. (2010).
882 High-affinity manganese uptake by the metal transporter NRAMP1 is
883 essential for Arabidopsis growth in low manganese conditions. *The*
884 *Plant cell* **22**, 904-917.
- 885 Castaings, L., Caquot, A., Loubet, S., and Curie, C. (2016). The high-
886 affinity metal Transporters NRAMP1 and IRT1 Team up to Take up Iron
887 under Sufficient Metal Provision. *Sci Rep* **6**, 37222.
- 888 Clough, S.J., and Bent, A.F. (1998). Floral dip: a simplified method for
889 Agrobacterium-mediated transformation of Arabidopsis thaliana. *Plant*
890 *J.* **16**, 735-743.
- 891 Cohen, A., Nelson, H., and Nelson, N. (2000). The Family of SMF Metal Ion
892 Transporters in Yeast Cells. *J. Biol. Chem.* **275**, 33388-33394.
- 893 Culotta, V.C., and Daly, M.J. (2013). Manganese complexes: diverse
894 metabolic routes to oxidative stress resistance in prokaryotes and
895 yeast. *Antioxid Redox Signal* **19**, 933-944.

896 Curie, C., Alonso, J.M., Le Jean, M., Ecker, J.R., and Briat, J.F. (2000).
897 Involvement of NRAMP1 from Arabidopsis thaliana in iron transport.
898 Biochem. J. 347, 749-755.

899 del Rio, L.A., Sandalio, L.M., Altomare, D.A., and Zilinskas, B.A. (2003).
900 Mitochondrial and peroxisomal manganese superoxide dismutase:
901 differential expression during leaf senescence. J Exp Bot 54, 923-
902 933.

903 Delhaize, E., Gruber, B.D., Pittman, J.K., White, R.G., Leung, H., Miao,
904 Y., Jiang, L., Ryan, P.R., and Richardson, A.E. (2007). A role for
905 the AtMTP11 gene of Arabidopsis in manganese transport and tolerance.
906 Plant J 51, 198-210.

907 Dinneny, J.R., Long, T.A., Wang, J.Y., Jung, J.W., Mace, D., Pointer, S.,
908 Barron, C., Brady, S.M., Schiefelbein, J., and Benfey, P.N. (2008).
909 Cell identity mediates the response of Arabidopsis roots to abiotic
910 stress. Science 320, 942-945.

911 Divol, F., Couch, D., Conejero, G., Roschzttardt, H., Mari, S., and Curie,
912 C. (2013). The Arabidopsis YELLOW STRIPE LIKE4 and 6 transporters
913 control iron release from the chloroplast. The Plant cell 25, 1040-
914 1055.

915 Domergue, F., Vishwanath, S.J., Joubes, J., Ono, J., Lee, J.A., Bourdon,
916 M., Alhattab, R., Lowe, C., Pascal, S., Lessire, R., and Rowland, O.
917 (2010). Three Arabidopsis fatty acyl-coenzyme A reductases, FAR1,
918 FAR4, and FAR5, generate primary fatty alcohols associated with
919 suberin deposition. Plant Physiol 153, 1539-1554.

920 Drakakaki, G., van de Ven, W., Pan, S., Miao, Y., Wang, J., Keinath, N.F.,
921 Weatherly, B., Jiang, L., Schumacher, K., Hicks, G., and Raikhel, N.
922 (2012). Isolation and proteomic analysis of the SYP61 compartment
923 reveal its role in exocytic trafficking in Arabidopsis. Cell Res 22,
924 413-424.

925 Eroglu, S., Meier, B., von Wiren, N., and Peiter, E. (2016). The Vacuolar
926 Manganese Transporter MTP8 Determines Tolerance to Iron Deficiency-
927 Induced Chlorosis in Arabidopsis. Plant Physiol 170, 1030-1045.

928 Foresti, O., Gershlick, D.C., Bottanelli, F., Hummel, E., Hawes, C., and
929 Denecke, J. (2010). A recycling-defective vacuolar sorting receptor
930 reveals an intermediate compartment situated between prevacuoles and
931 vacuoles in tobacco. Plant Cell 22, 3992-4008.

932 Garcia-Rodriguez, N., Diaz de la Loza Mdel, C., Andreson, B., Monje-Casas,
933 F., Rothstein, R., and Wellinger, R.E. (2012). Impaired manganese
934 metabolism causes mitotic misregulation. J Biol Chem 287, 18717-
935 18729.

936 Garcia-Rodriguez, N., Manzano-Lopez, J., Munoz-Bravo, M., Fernandez-Garcia,
937 E., Muniz, M., and Wellinger, R.E. (2015). Manganese redistribution
938 by calcium-stimulated vesicle trafficking bypasses the need for P-
939 type ATPase function. J Biol Chem 290, 9335-9347.

940 Geldner, N., Denervaud-Tendon, V., Hyman, D.L., Mayer, U., Stierhof, Y.D.,
941 and Chory, J. (2009). Rapid, combinatorial analysis of membrane
942 compartments in intact plants with a multicolor marker set. Plant J
943 59, 169-178.

944 Heberlein, C.A., Laursen, K.H., Ladegaard, A.H., Schmidt, S.B., Pedas, P.,
945 Bruhn, D., Schjoerring, J.K., Wulfsohn, D., and Husted, S. (2009).
946 Latent manganese deficiency increases transpiration in barley
947 (Hordeum vulgare). Physiol Plant 135, 307-316.

948 Hoffmann-Benning, S., and Kende, H. (1994). Cuticle Biosynthesis in Rapidly
949 Growing Internodes of Deepwater Rice. Plant Physiol 104, 719-723.

950 Ishimaru, Y., Takahashi, R., Bashir, K., Shimo, H., Senoura, T., Sugimoto,
951 K., Ono, K., Yano, M., Ishikawa, S., Arao, T., Nakanishi, H., and
952 Nishizawa, N.K. (2012). Characterizing the role of rice NRAMP5 in
953 Manganese, Iron and Cadmium Transport. Sci Rep 2, 286.

954 Kim, S.A., Punshon, T., Lanzirotti, A., Li, L., Alonso, J.M., Ecker, J.R.,
955 Kaplan, J., and Gueriot, M.L. (2006). Localization of iron in

956 Arabidopsis seed requires the vacuolar membrane transporter VIT1.
957 Science **314**, 1295-1298.

958 Lanquar, V., Ramos, M.S., Lelievre, F., Barbier-Brygoo, H., Krieger-
959 Liskay, A., Kramer, U., and Thomine, S. (2010). Export of vacuolar
960 manganese by AtNRAMP3 and AtNRAMP4 is required for optimal
961 photosynthesis and growth under manganese deficiency. Plant Physiol
962 **152**, 1986-1999.

963 Lanquar, V., Lelievre, F., Bolte, S., Hames, C., Alcon, C., Neumann, D.,
964 Vansuyt, G., Curie, C., Schroder, A., Kramer, U., Barbier-Brygoo, H.,
965 and Thomine, S. (2005). Mobilization of vacuolar iron by AtNRAMP3 and
966 AtNRAMP4 is essential for seed germination on low iron. Embo J **24**,
967 4041-4051.

968 Lin, Y.T., Hoang, H., Hsieh, S.I., Rangel, N., Foster, A.L., Sampayo, J.N.,
969 Lithgow, G.J., and Srinivasan, C. (2006). Manganous ion
970 supplementation accelerates wild type development, enhances stress
971 resistance, and rescues the life span of a short-lived Caenorhabditis
972 elegans mutant. Free Radic Biol Med **40**, 1185-1193.

973 Luk, E., Carroll, M., Baker, M., and Culotta, V.C. (2003). Manganese
974 activation of superoxide dismutase 2 in Saccharomyces cerevisiae
975 requires MTM1, a member of the mitochondrial carrier family. Proc
976 Natl Acad Sci U S A **100**, 10353-10357.

977 Luk, E.E., and Culotta, V.C. (2001). Manganese Superoxide Dismutase in
978 Saccharomyces cerevisiae Acquires Its Metal Co-factor through a
979 Pathway Involving the Nramp Metal Transporter, Smf2p. J Biol Chem
980 **276**, 47556-47562.

981 Marschner, H., Romheld, V., and Kissel, M. (1986). Different strategies in
982 higher plants in mobilization and uptake of iron. J. Plant Nutr. **9**,
983 3-7.

984 Martiniere, A., Bassil, E., Jublanc, E., Alcon, C., Reguera, M., Sentenac,
985 H., Blumwald, E., and Paris, N. (2013). In vivo intracellular pH
986 measurements in tobacco and Arabidopsis reveal an unexpected pH
987 gradient in the endomembrane system. Plant Cell **25**, 4028-4043.

988 McNaughton, R.L., Reddi, A.R., Clement, M.H., Sharma, A., Barnese, K.,
989 Rosenfeld, L., Gralla, E.B., Valentine, J.S., Culotta, V.C., and
990 Hoffman, B.M. (2010). Probing in vivo Mn²⁺ speciation and oxidative
991 stress resistance in yeast cells with electron-nuclear double
992 resonance spectroscopy. Proc Natl Acad Sci U S A **107**, 15335-15339.

993 Mills, R.F., Doherty, M.L., Lopez-Marques, R.L., Weimar, T., Dupree, P.,
994 Palmgren, M.G., Pittman, J.K., and Williams, L.E. (2008). ECA3, a
995 Golgi-localized P2A-type ATPase, plays a crucial role in manganese
996 nutrition in Arabidopsis. Plant Physiol **146**, 116-128.

997 Milner, M.J., Seamon, J., Craft, E., and Kochian, L.V. (2013). Transport
998 properties of members of the ZIP family in plants and their role in
999 Zn and Mn homeostasis. J Exp Bot **64**, 369-381.

1000 Momonoi, K., Yoshida, K., Mano, S., Takahashi, H., Nakamori, C., Shoji, K.,
1001 Nitta, A., and Nishimura, M. (2009). A vacuolar iron transporter in
1002 tulip, TgVIT1, is responsible for blue coloration in petal cells
1003 through iron accumulation. Plant J **59**, 437-447.

1004 Nelson, N., Sacher, A., and Nelson, H. (2002). The significance of
1005 molecular slips in transport systems. Nat Rev Mol Cell Biol **3**, 876-
1006 881.

1007 Nevo, Y., and Nelson, N. (2006). The NRAMP family of metal-ion
1008 transporters. Biochim Biophys Acta **1763**, 609-620.

1009 Nickelsen, J., and Rengstl, B. (2013). Photosystem II assembly: from
1010 cyanobacteria to plants. Annu Rev Plant Biol **64**, 609-635.

1011 Pedas, P., Schiller Stockholm, M., Hegelund, J.N., Ladegard, A.H.,
1012 Schjoerring, J.K., and Husted, S. (2014). Golgi localized barley MTP8
1013 proteins facilitate Mn transport. PLoS One **9**, e113759.

1014 Peiter, E., Montanini, B., Gobert, A., Pedas, P., Husted, S., Maathuis,
1015 F.J., Blaudez, D., Chalot, M., and Sanders, D. (2007). A secretory

1016 pathway-localized cation diffusion facilitator confers plant
1017 manganese tolerance. *Proc Natl Acad Sci U S A* **104**, 8532-8537.

1018 **Pittman, J.K., Shigaki, T., Marshall, J.L., Morris, J.L., Cheng, N.H., and**
1019 **Hirschi, K.D.** (2004). Functional and regulatory analysis of the
1020 *Arabidopsis thaliana* CAX2 cation transporter. *Plant Mol Biol* **56**, 959-
1021 971.

1022 **Portnoy, M.E., Liu, X.F., and Culotta, V.C.** (2000). *Saccharomyces*
1023 *cerevisiae* expresses three functionally distinct homologues of the
1024 nramp family of metal transporters. *Mol. Cell. Biol.* **20**, 7893-7902.

1025 **Ravet, K., Touraine, B., Kim, S.A., Cellier, F., Thomine, S., Guerinot,**
1026 **M.L., Briat, J.F., and Gaymard, F.** (2009). Post-translational
1027 regulation of AtFER2 ferritin in response to intracellular iron
1028 trafficking during fruit development in *Arabidopsis*. *Mol Plant* **2**,
1029 1095-1106.

1030 **Roth, J.A.** (2006). Homeostatic and toxic mechanisms regulating manganese
1031 uptake, retention, and elimination. *Biol Res* **39**, 45-57.

1032 **Rudolph, H.K., Antebi, A., Fink, G.R., Buckley, C.M., Dorman, T.E.,**
1033 **LeVitre, J., Davidow, L.S., Mao, J.I., and Moir, D.T.** (1989). The
1034 yeast secretory pathway is perturbed by mutations in PMR1, a member
1035 of a Ca²⁺ ATPase family. *Cell* **58**, 133-145.

1036 **Sasaki, A., Yamaji, N., Yokosho, K., and Ma, J.F.** (2012). Nramp5 is a major
1037 transporter responsible for manganese and cadmium uptake in rice.
1038 *Plant Cell* **24**, 2155-2167.

1039 **Schmidt, S.B., Jensen, P.E., and Husted, S.** (2016). Manganese Deficiency in
1040 Plants: The Impact on Photosystem II. *Trends Plant Sci* **21**, 622-632.

1041 **Schneider, A., Steinberger, I., Herdean, A., Gandini, C., Eisenhut, M.,**
1042 **Kurz, S., Morper, A., Hoecker, N., Ruhle, T., Labs, M., Flugge, U.I.,**
1043 **Geimer, S., Schmidt, S.B., Husted, S., Weber, A.P., Spetea, C., and**
1044 **Leister, D.** (2016). The Evolutionarily Conserved Protein
1045 PHOTOSYNTHESIS AFFECTED MUTANT71 Is Required for Efficient Manganese
1046 Uptake at the Thylakoid Membrane in *Arabidopsis*. *Plant Cell* **28**, 892-
1047 910.

1048 **Su, Z., Chai, M.F., Lu, P.L., An, R., Chen, J., and Wang, X.C.** (2007).
1049 AtMTM1, a novel mitochondrial protein, may be involved in activation
1050 of the manganese-containing superoxide dismutase in *Arabidopsis*.
1051 *Planta* **226**, 1031-1039.

1052 **Supek, F., Supekova, L., Nelson, H., and Nelson, N.** (1996). A yeast
1053 manganese transporter related to the macrophage protein involved in
1054 conferring resistance to mycobacteria. *Proc. Natl Acad. Sci. U. S. A.*
1055 **93**, 5105-5110.

1056 **Tanaka, T., Tanaka, H., Machida, C., Watanabe, M., and Machida, Y.** (2004).
1057 A new method for rapid visualization of defects in leaf cuticle
1058 reveals five intrinsic patterns of surface defects in *Arabidopsis*.
1059 *Plant J* **37**, 139-146.

1060 **Techau, M.E., Valdez-Taubas, J., Popoff, J.F., Francis, R., Seaman, M., and**
1061 **Blackwell, J.M.** (2007). Evolution of differences in transport
1062 function in Slc11a family members. *J Biol Chem* **282**, 35646-35656.

1063 **Thomine, S., Wang, R., Ward, J.M., Crawford, N.M., and Schroeder, J.I.**
1064 (2000). Cadmium and iron transport by members of a plant metal
1065 transporter family in *Arabidopsis* with homology to Nramp genes. *Proc.*
1066 *Natl Acad. Sci. U. S. A.* **97**, 4991-4996.

1067 **Uemura, T., and Nakano, A.** (2013). Plant TGNs: dynamics and physiological
1068 functions. *Histochem Cell Biol* **140**, 341-345.

1069 **Whittaker, M.M., Penmatsa, A., and Whittaker, J.W.** (2015). The Mtm1p
1070 carrier and pyridoxal 5'-phosphate cofactor trafficking in yeast
1071 mitochondria. *Arch Biochem Biophys* **568**, 64-70.

1072 **Wilson, D.O., Boswell, F.C., Ohki, K., Parker, M.B., Shuman, L.M., and**
1073 **Jellum, M.D.** (1982). Changes in soybean seed oil and protein as
1074 influenced by manganese nutrition. *Crop Science* **22**, 948-952.

1075 **Wu, Z., Liang, F., Hong, B., Young, J.C., Sussman, M.R., Harper, J.F., and**
1076 **Sze, H.** (2002). An endoplasmic reticulum-bound Ca(2+)/Mn(2+) pump,

1077 ECA1, supports plant growth and confers tolerance to Mn(2+) stress.
1078 Plant Physiol **130**, 128-137.
1079 **Yang, M., Cobine, P.A., Molik, S., Naranuntarat, A., Lill, R., Winge, D.R.,**
1080 **and Culotta, V.C.** (2006). The effects of mitochondrial iron
1081 homeostasis on cofactor specificity of superoxide dismutase 2. *Embo J*
1082 **25**, 1775-1783.
1083 **Yeats, T.H., and Rose, J.K.** (2013). The formation and function of plant
1084 cuticles. *Plant Physiol* **163**, 5-20.
1085 **Zhang, Y., Xu, Y.H., Yi, H.Y., and Gong, J.M.** (2012). Vacuolar membrane
1086 transporters OsVIT1 and OsVIT2 modulate iron translocation between
1087 flag leaves and seeds in rice. *Plant J* **72**, 400-410.
1088

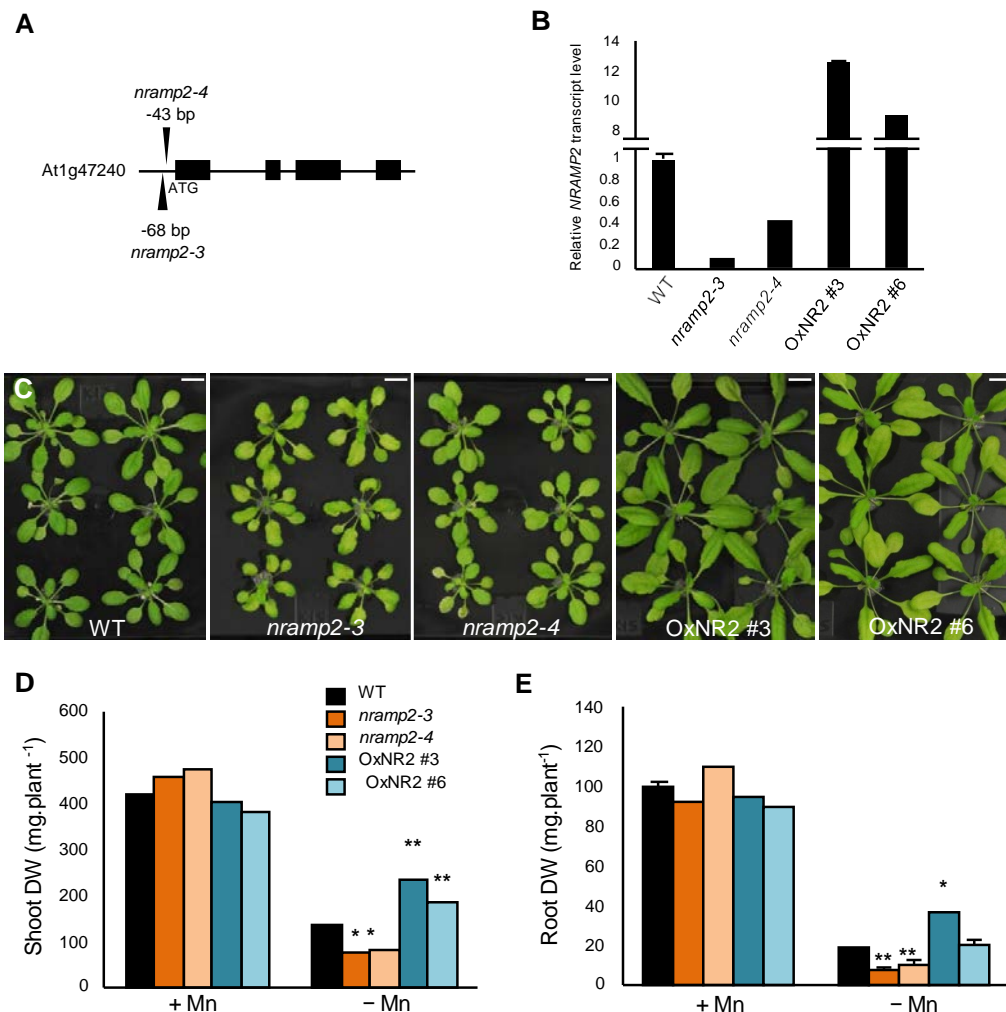


Figure 1. *nramp2* mutants are hypersensitive to Mn deficiency.

(A) Position relative to the ATG start codon of the T-DNA insertion in two *nramp2* mutant alleles.

(B) Relative *NRAMP2* transcript abundance measured by qRT-PCR in *nramp2-3* mutant alleles and in the two *nramp2-3* complemented lines OxNR2 #3 and OxNR2 #6. Transcripts levels are expressed relative to those of the reference gene ACTIN \pm SD ($n=3$ technical replicates). **(C)** Phenotype of the indicated genetic backgrounds grown for one week in Mn-replete conditions ($5 \mu\text{M}$ Mn SO_4) followed by 3 additional weeks in Mn-free hydroponic conditions.

(D) and **(E)** Shoot **(D)** and root **(E)** biomass production of the plants presented in C (-Mn) or in Mn replete conditions (Control). Data are from one representative experiment ($n = 10$ plants). Panels D and E share color code legends. Mean \pm SD. Asterisks indicate values statistically different from those of wild type (Student's *t* test, * P -value < 0.05 , ** P -value < 0.01). Scale bar = 1 cm.

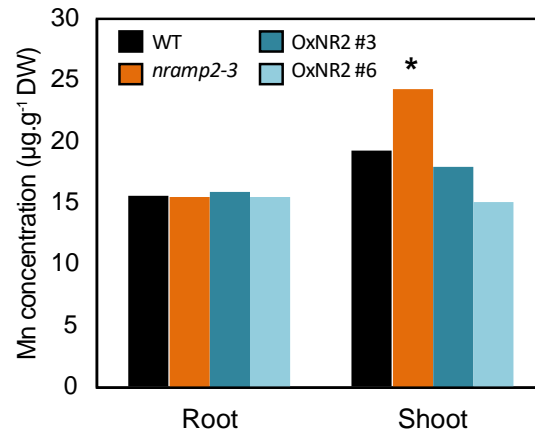


Figure 2. *nramp2-3* shows Mn homeostasis defects under Mn-free conditions.

(A) Mn content in the plants presented in Figure 1 and in control plants grown in parallel in Mn-replete conditions Supplemental Figure 1D. Data are from one representative experiment (n = 4 plants). DW: Dry weight. Mean ± sd. Asterisks indicate values statistically different from those of wild type (Student's *t* test, * P-value < 0.01).

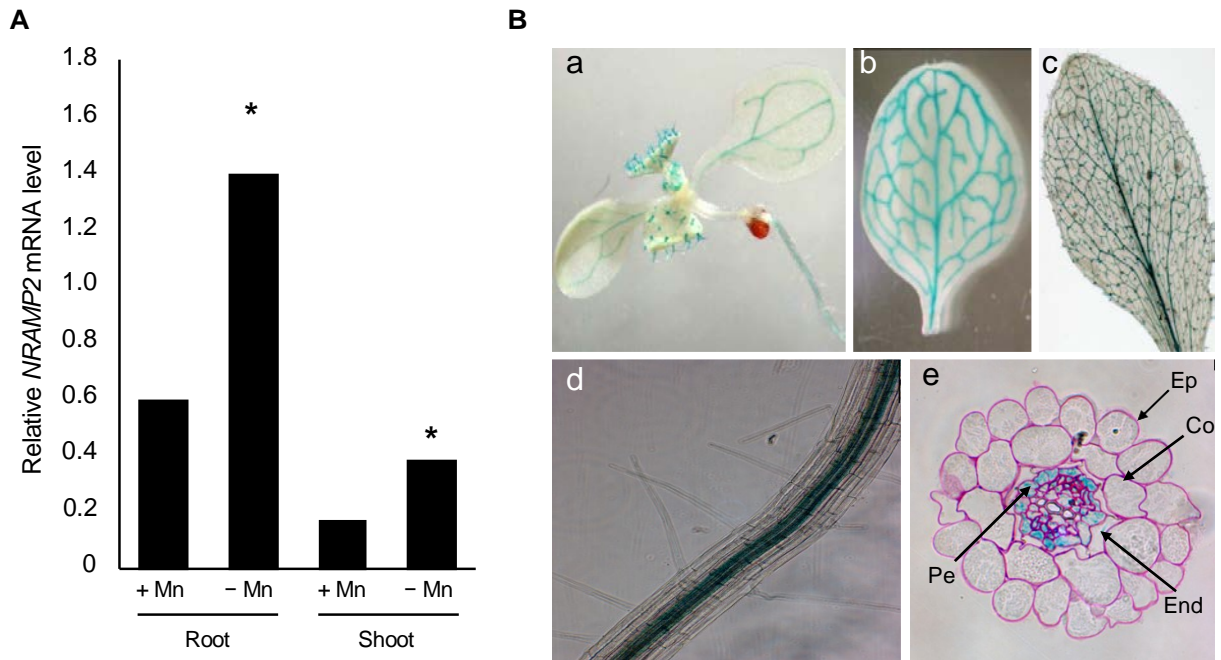


Figure 3. *NRAMP2* gene expression analysis.

(A) Relative *NRAMP2* transcripts abundance in roots and shoot measured by qRT-PCR. Transcripts levels are expressed relative to those of the reference gene *ACTIN* \pm SD (n=3 technical replicates). Wild-type plants were grown hydroponically for 3 weeks in control (5 μ M MnSO₄) or in Mn-free (-Mn) conditions. Data are from one representative experiment (n = 3 plants). Mean \pm SD. Asterisks indicate values statistically different from those of control conditions (Student's *t* test, * P-value < 0.01).

(B) Histochemical staining of GUS activity in p*NRAMP2*::GUS-transformed *Arabidopsis* grown in Mn-replete conditions. (a) 6 day-old seedling. (b) Young rosette leaf. (c) Mature rosette leaf. (d) Primary root of a one week-old plant in the mature zone. (e) Root cross-section in the mature zone. Ep: epidermis, Co: cortex, End: endodermis, Pe: pericycle. Data are shown for one representative line out of 3 independent lines.

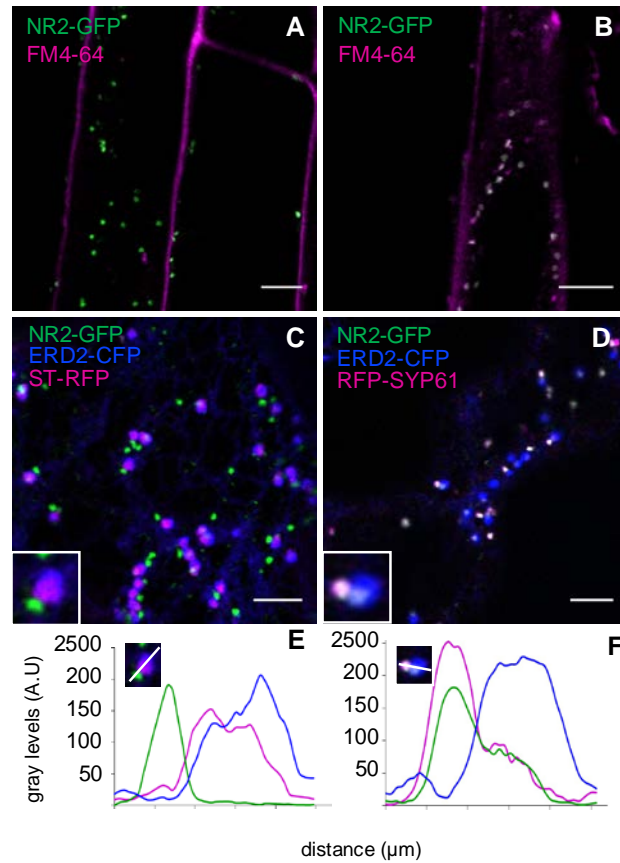


Figure 4. NRAMP2 is localized in Trans-Golgi Network.

(A) and (B) Fluorescence pattern of the NRAMP2-GFP construct and kinetics of colocalization with the endocytic tracer FM4-64 (A: 2 min, B: 15 min) observed by confocal microscopy in roots of 5-day old plants.

(C) and (D) Colocalization of NRAMP2-GFP with markers for cis-Golgi (ERD2-CFP), trans-Golgi (ST-RFP), TGN (RFP-SYP61), transiently co-expressed in tobacco leaves. Inserts show a close-up image of the association of NRAMP2-GFP with the various Golgi subcompartments. Scale bars : 5 μm

(E) and (F) pixel intensity profiles of GFP (green), RFP (magenta) and CFP (blue) were measured along a line spanning the sub-compartments magnified in the close-up inserts (C) and (D) respectively.

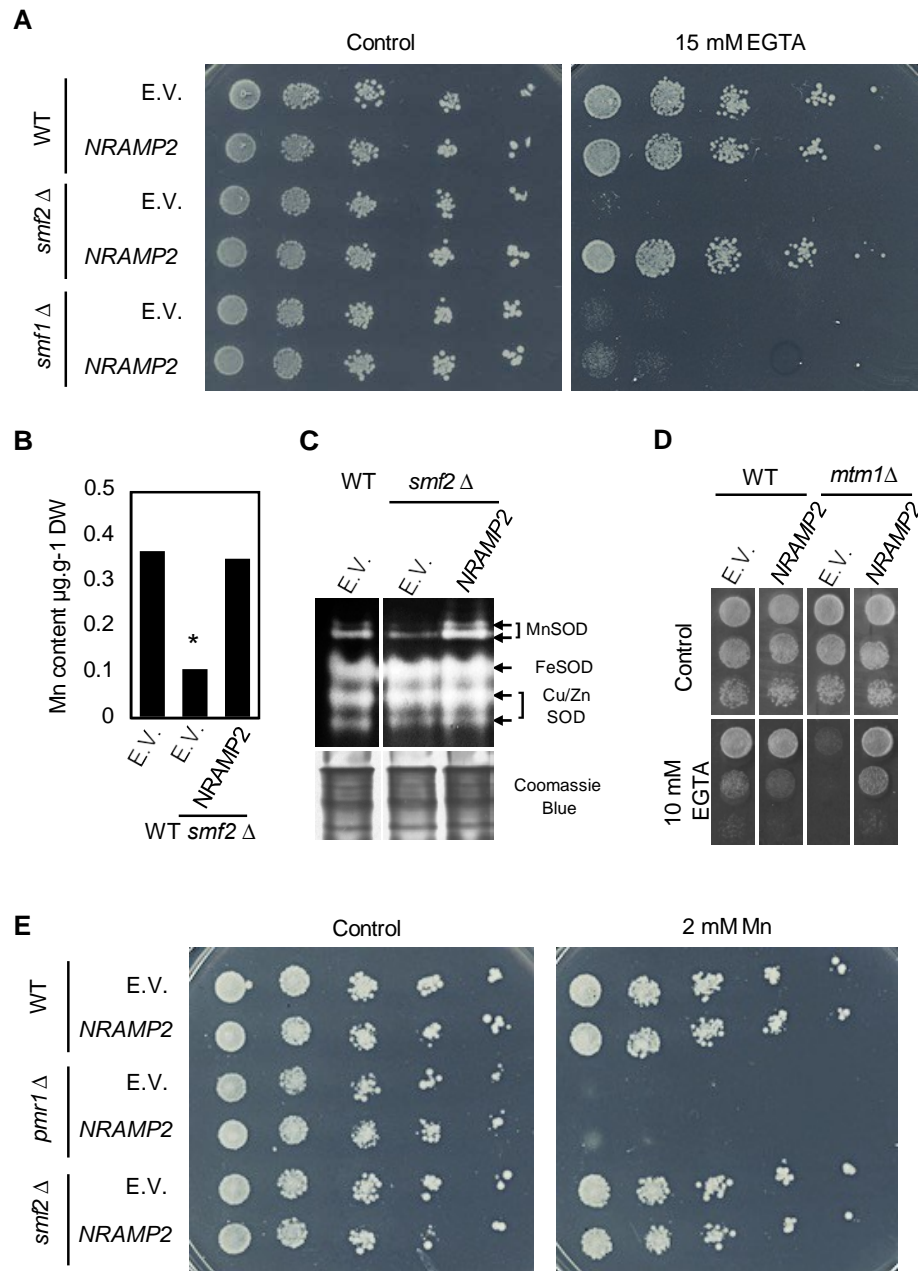


Figure 5. NRAMP2 complements *smf2*Δ and *mtm1*Δ yeast mutants.

(A), (D) and (E) Growth tests of wild type (BY4741) and either one of the mutant yeast strains *smf1*Δ (A), *smf2*Δ (A,E), *mtm1*Δ (D) and *pmr1*Δ (E) transformed with the pYPGE15 empty vector (E.V.) or the pYPGE15/NRAMP2 construct (NRAMP2). 5-fold serial dilutions were plated on SD-Ura supplemented or not (control) with the amount of EGTA indicated on the Figure panels (A, D) or 2mM MnSO₄ (E) and incubated at 30°C for 3 days.

(A) NRAMP2 restores *smf2*Δ mutant tolerance to Mn deficiency.

(B) Mn content measured by MP-AES in yeast strains grown in liquid SD -URA for 24 hours. Mean ± SD.

Asterisks indicate values statistically different from those of wild type (Student's *t* test, * P-value < 0.01).

(C) *In gel* SOD activity carried out on proteins extracted from yeast strains grown as in (B).

(D) NRAMP2 restores *mtm1*Δ mutant tolerance to Mn deficiency.

(E) NRAMP2 fails to rescue *pmr1*Δ mutant sensitivity to Mn excess and does not reduce wild-type or *smf2*Δ tolerance to Mn excess.

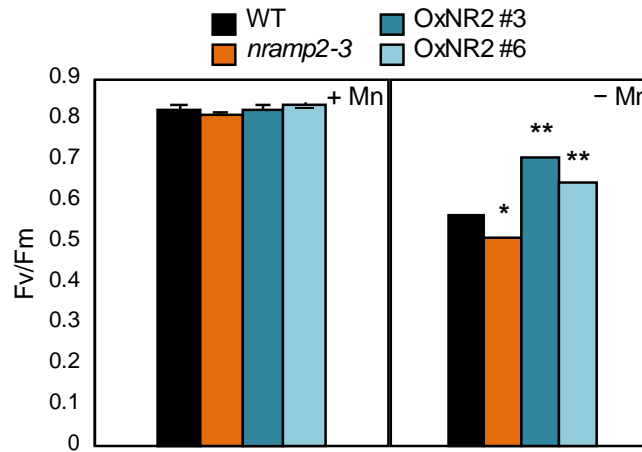


Figure 6. Photosynthetic activity is impaired in *nramp2-3*.

Maximum PSII efficiency (Fv/Fm) measured on rosette leaves of wild-type, *nramp2-3* and two complemented lines grown either for 4 weeks in hydroponic conditions in the presence of Mn (+Mn) or 1 week with Mn and transferred without Mn for 3 additional weeks (-Mn). Mean \pm SD (n = 10 leaves from 10 plants). Asterisks indicate values statistically different from those of wild type (Student's *t* test, * P-value < 0.05, ** P-value < 0.01).

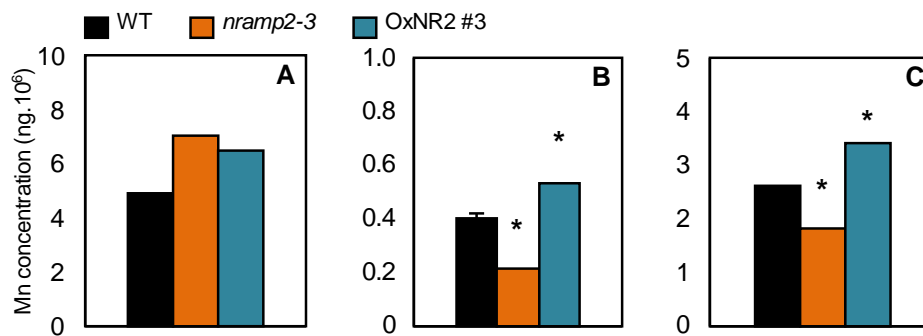


Figure 7. Vacuoles and chloroplasts of the *nramp2-3* mutant contain less Mn. **(A)** to **(C)** Mn content was measured on isolated protoplasts **(A)**, chloroplasts **(B)** or vacuoles **(C)** in wild-type, *nramp2-3* and the OxNR2 #3 complemented line grown in hydroponic cultures for one week in the presence of Mn followed by three additional weeks in the absence of Mn. All panels share color code legends. Metal concentration was determined by MP-AES and is expressed as ng per 10⁶ protoplasts or organelles. Data are from one representative experiment (n = 4 plants). Mean ± SD. Asterisks indicate values statistically different from those of wild type (Student's *t* test, * P-value < 0.01).

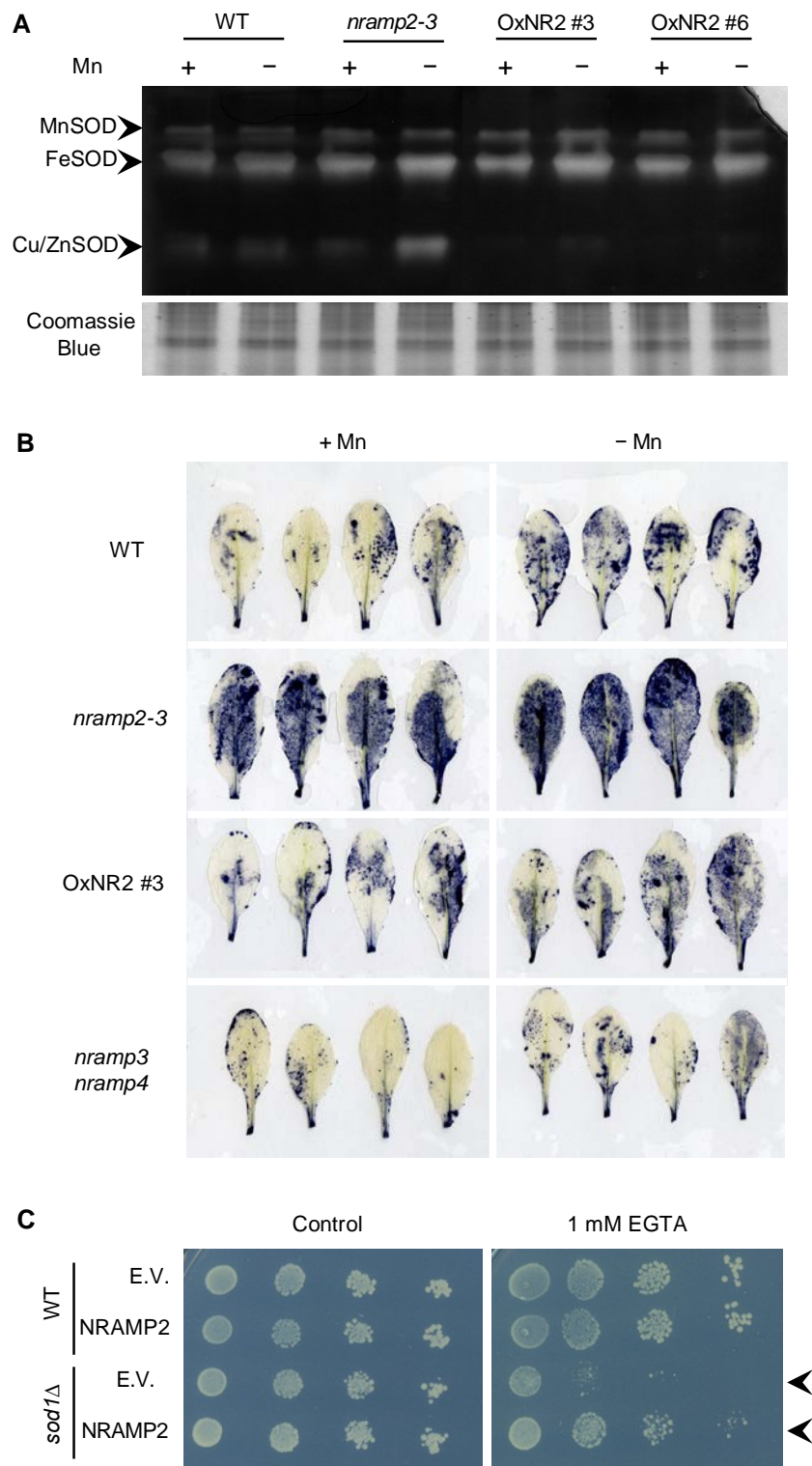


Figure 8. *nramp2-3* displays high oxidative stress.

(A) and (B) Plants of the indicated genotypes were cultivated in hydroponic conditions for 4 weeks in hydroponic conditions in the presence of Mn (+Mn) or 1 week with Mn and transferred without Mn for 3 additional weeks (-Mn). (A) In-gel SOD activity performed using total proteins extracted from leaves. (B) Detection of superoxide ions production in Mn replete or Mn-starved leaves by staining with nitroblue tetrazolium (NBT). (C) NRAMP2 rescues sensitivity of the yeast *sod1Δ* mutant to Mn deficiency. 5-fold serial dilutions were plated on SD-Ura supplemented with 1 mM EGTA (right) or not (Control, left).

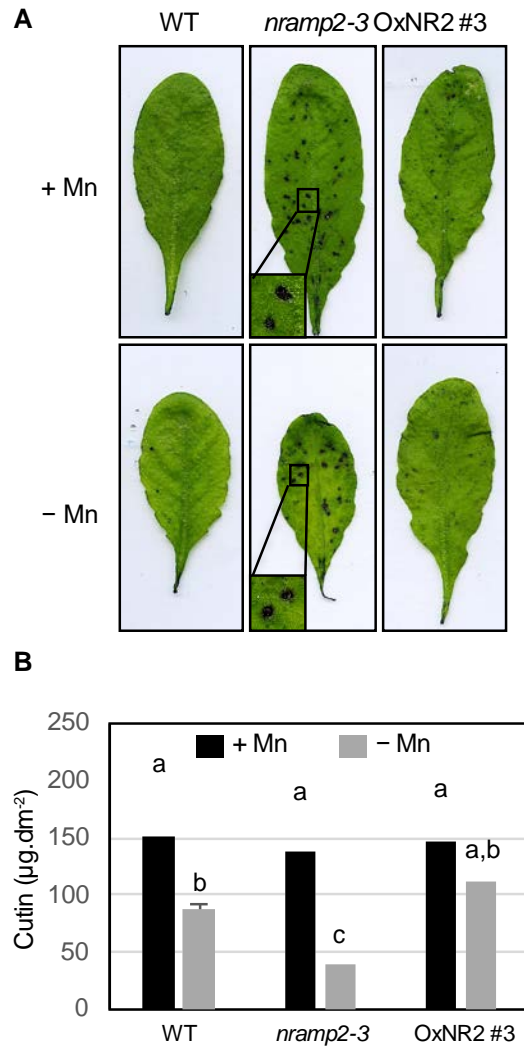


Figure 9. *nramp2-3* shows cell wall permeability defects.

Plants of the indicated genotypes were grown in hydroponic conditions for 3 weeks in the presence of Mn followed by an additional week either in Mn (+ Mn) or in the absence of Mn (-Mn).

(A) Permeability of the leaf surface was examined by staining entire leaves with Toluidine blue for 10 min. Inserts show a closeup view of the TB-stained spots on the leaves.

(B) Cutin load per surface unit of leaf measured by GC-MS. Mean \pm SD (n= 4 leaves from 4 plants). Values that are not statistically different are noted with the same letter (ANOVA, α risk 5%).

Parsed Citations

Agorio, A., Giraudat, J., Bianchi, M.W., Marion, J., Espagne, C., Castaings, L., Lelievre, F., Curie, C., Thomine, S., and Merlot, S. (2017). Phosphatidylinositol 3-phosphate-binding protein AtPH1 controls the localization of the metal transporter NRAMP1 in Arabidopsis. *Proc Natl Acad Sci U S A* 114, E3354-E3363.

Pubmed: [Author and Title](#)

CrossRef: [Author and Title](#)

Google Scholar: [Author Only Title Only Author and Title](#)

Allen, M.D., Kropat, J., Tottey, S., Del Campo, J.A., and Merchant, S.S. (2007). Manganese deficiency in Chlamydomonas results in loss of photosystem II and MnSOD function, sensitivity to peroxides, and secondary phosphorus and iron deficiency. *Plant Physiol* 143, 263-277.

Pubmed: [Author and Title](#)

CrossRef: [Author and Title](#)

Google Scholar: [Author Only Title Only Author and Title](#)

Barberon, M., Vermeer, J.E., De Bellis, D., Wang, P., Naseer, S., Andersen, T.G., Humbel, B.M., Nawrath, C., Takano, J., Salt, D.E., and Geldner, N. (2016). Adaptation of root function by nutrient-induced plasticity of endodermal differentiation. *Cell* 164, 447-459.

Pubmed: [Author and Title](#)

CrossRef: [Author and Title](#)

Google Scholar: [Author Only Title Only Author and Title](#)

Bolte, S., and Cordelieres, F.P. (2006). A guided tour into subcellular colocalization analysis in light microscopy. *J Microsc* 224, 213-232.

Pubmed: [Author and Title](#)

CrossRef: [Author and Title](#)

Google Scholar: [Author Only Title Only Author and Title](#)

Brandizzi, F., Frangne, N., Marc-Martin, S., Hawes, C., Neuhaus, J.M., and Paris, N. (2002). The destination for single-pass membrane proteins is influenced markedly by the length of the hydrophobic domain. *Plant Cell* 14, 1077-1092.

Pubmed: [Author and Title](#)

CrossRef: [Author and Title](#)

Google Scholar: [Author Only Title Only Author and Title](#)

Cailliatte, R., Lapeyre, B., Briat, J.F., Mari, S., and Curie, C. (2009). The NRAMP6 metal transporter contributes to cadmium toxicity. *Biochem J* 422, 217-228.

Pubmed: [Author and Title](#)

CrossRef: [Author and Title](#)

Google Scholar: [Author Only Title Only Author and Title](#)

Cailliatte, R., Schikora, A., Briat, J.F., Mari, S., and Curie, C. (2010). High-affinity manganese uptake by the metal transporter NRAMP1 is essential for Arabidopsis growth in low manganese conditions. *The Plant cell* 22, 904-917.

Pubmed: [Author and Title](#)

CrossRef: [Author and Title](#)

Google Scholar: [Author Only Title Only Author and Title](#)

Castaings, L., Caquot, A., Loubet, S., and Curie, C. (2016). The high-affinity metal Transporters NRAMP1 and IRT1 Team up to Take up Iron under Sufficient Metal Provision. *Sci Rep* 6, 37222.

Pubmed: [Author and Title](#)

CrossRef: [Author and Title](#)

Google Scholar: [Author Only Title Only Author and Title](#)

Clough, S.J., and Bent, A.F. (1998). Floral dip: a simplified method for Agrobacterium-mediated transformation of Arabidopsis thaliana. *Plant J.* 16, 735-743.

Pubmed: [Author and Title](#)

CrossRef: [Author and Title](#)

Google Scholar: [Author Only Title Only Author and Title](#)

Cohen, A., Nelson, H., and Nelson, N. (2000). The Family of SMF Metal Ion Transporters in Yeast Cells. *J. Biol. Chem.* 275, 33388-33394.

Pubmed: [Author and Title](#)

CrossRef: [Author and Title](#)

Google Scholar: [Author Only Title Only Author and Title](#)

Culotta, V.C., and Daly, M.J. (2013). Manganese complexes: diverse metabolic routes to oxidative stress resistance in prokaryotes and yeast. *Antioxid Redox Signal* 19, 933-944.

Pubmed: [Author and Title](#)

CrossRef: [Author and Title](#)

Google Scholar: [Author Only Title Only Author and Title](#)

Curie, C., Alonso, J.M., Le Jean, M., Ecker, J.R., and Briat, J.F. (2000). Involvement of NRAMP1 from Arabidopsis thaliana in iron transport. *Biochem. J.* 347, 749-755.

Pubmed: [Author and Title](#)

CrossRef: [Author and Title](#)

Google Scholar: [Author Only Title Only Author and Title](#)

del Rio, L.A., Sandalio, L.M., Altomare, D.A., and Zilinskas, B.A. (2003). Mitochondrial and peroxisomal manganese superoxide dismutase: differential expression during leaf senescence. *J Exp Bot* 54, 923-933.

Pubmed: [Author and Title](#)

CrossRef: [Author and Title](#)

Google Scholar: [Author Only Title Only Author and Title](#)

Delhaize, E., Gruber, B.D., Pittman, J.K., White, R.G., Leung, H., Miao, Y., Jiang, L., Ryan, P.R., and Richardson, A.E. (2007). Arole for the AtMTP11 gene of Arabidopsis in manganese transport and tolerance. *Plant J* 51, 198-210.

Pubmed: [Author and Title](#)

CrossRef: [Author and Title](#)

Google Scholar: [Author Only Title Only Author and Title](#)

Dinneny, J.R., Long, T.A., Wang, J.Y., Jung, J.W., Mace, D., Pointer, S., Barron, C., Brady, S.M., Schiefelbein, J., and Benfey, P.N. (2008). Cell identity mediates the response of Arabidopsis roots to abiotic stress. *Science* 320, 942-945.

Pubmed: [Author and Title](#)

CrossRef: [Author and Title](#)

Google Scholar: [Author Only Title Only Author and Title](#)

Divol, F., Couch, D., Conejero, G., Roschztardt, H., Mari, S., and Curie, C. (2013). The Arabidopsis YELLOWSTRIPE LIKE4 and 6 transporters control iron release from the chloroplast. *The Plant cell* 25, 1040-1055.

Pubmed: [Author and Title](#)

CrossRef: [Author and Title](#)

Google Scholar: [Author Only Title Only Author and Title](#)

Domergue, F., Vishwanath, S.J., Joubes, J., Ono, J., Lee, J.A., Bourdon, M., Alhattab, R., Lowe, C., Pascal, S., Lessire, R., and Rowland, O. (2010). Three Arabidopsis fattyacyl-coenzyme A reductases, FAR1, FAR4, and FAR5, generate primary fatty alcohols associated with suberin deposition. *Plant Physiol* 153, 1539-1554.

Pubmed: [Author and Title](#)

CrossRef: [Author and Title](#)

Google Scholar: [Author Only Title Only Author and Title](#)

Drakakaki, G., van de Ven, W., Pan, S., Miao, Y., Wang, J., Keinath, N.F., Weatherly, B., Jiang, L., Schumacher, K., Hicks, G., and Raikhel, N. (2012). Isolation and proteomic analysis of the SYP61 compartment reveal its role in exocytic trafficking in Arabidopsis. *Cell Res* 22, 413-424.

Pubmed: [Author and Title](#)

CrossRef: [Author and Title](#)

Google Scholar: [Author Only Title Only Author and Title](#)

Eroglu, S., Meier, B., von Wiren, N., and Peiter, E. (2016). The Vacuolar Manganese Transporter MTP8 Determines Tolerance to Iron Deficiency-Induced Chlorosis in Arabidopsis. *Plant Physiol* 170, 1030-1045.

Pubmed: [Author and Title](#)

CrossRef: [Author and Title](#)

Google Scholar: [Author Only Title Only Author and Title](#)

Foresti, O., Gershlick, D.C., Bottanelli, F., Hummel, E., Hawes, C., and Denecke, J. (2010). A recycling-defective vacuolar sorting receptor reveals an intermediate compartment situated between prevacuoles and vacuoles in tobacco. *Plant Cell* 22, 3992-4008.

Pubmed: [Author and Title](#)

CrossRef: [Author and Title](#)

Google Scholar: [Author Only Title Only Author and Title](#)

Garcia-Rodriguez, N., Diaz de la Loza Mdel, C., Andreson, B., Monje-Casas, F., Rothstein, R., and Wellinger, R.E. (2012). Impaired manganese metabolism causes mitotic misregulation. *J Biol Chem* 287, 18717-18729.

Pubmed: [Author and Title](#)

CrossRef: [Author and Title](#)

Google Scholar: [Author Only Title Only Author and Title](#)

Garcia-Rodriguez, N., Manzano-Lopez, J., Munoz-Bravo, M., Fernandez-Garcia, E., Muniz, M., and Wellinger, R.E. (2015). Manganese redistribution by calcium-stimulated vesicle trafficking bypasses the need for P-type ATPase function. *J Biol Chem* 290, 9335-9347.

Pubmed: [Author and Title](#)

CrossRef: [Author and Title](#)

Google Scholar: [Author Only Title Only Author and Title](#)

Geldner, N., Denervaud-Tendon, V., Hyman, D.L., Mayer, U., Stierhof, Y.D., and Chory, J. (2009). Rapid, combinatorial analysis of membrane compartments in intact plants with a multicolor marker set. *Plant J* 59, 169-178.

Pubmed: [Author and Title](#)

CrossRef: [Author and Title](#)

Google Scholar: [Author Only Title Only Author and Title](#)

Hebborn, C.A., Laursen, K.H., Ladegaard, A.H., Schmidt, S.B., Pedas, P., Bruhn, D., Schjoerring, J.K., Wulfsohn, D., and Husted, S. (2009). Latent manganese deficiency increases transpiration in barley (*Hordeum vulgare*). *Physiol Plant* 135, 307-316.

Pubmed: [Author and Title](#)

CrossRef: [Author and Title](#)

Google Scholar: [Author Only Title Only Author and Title](#)

Hoffmann-Benning, S., and Kende, H. (1994). Cuticle Biosynthesis in Rapidly Growing Internodes of Deepwater Rice. *Plant Physiol* 104,

719-723.

Pubmed: [Author and Title](#)

CrossRef: [Author and Title](#)

Google Scholar: [Author Only Title Only Author and Title](#)

Ishimaru, Y., Takahashi, R., Bashir, K., Shimo, H., Senoura, T., Sugimoto, K., Ono, K., Yano, M., Ishikawa, S., Arao, T., Nakanishi, H., and Nishizawa, N.K. (2012). Characterizing the role of rice NRAMP5 in Manganese, Iron and Cadmium Transport. *Sci Rep* 2, 286.

Pubmed: [Author and Title](#)

CrossRef: [Author and Title](#)

Google Scholar: [Author Only Title Only Author and Title](#)

Kim, S.A., Punshon, T., Lanzirotti, A., Li, L., Alonso, J.M., Ecker, J.R., Kaplan, J., and Guerinot, M.L. (2006). Localization of iron in Arabidopsis seed requires the vacuolar membrane transporter VIT1. *Science* 314, 1295-1298.

Pubmed: [Author and Title](#)

CrossRef: [Author and Title](#)

Google Scholar: [Author Only Title Only Author and Title](#)

Lanquar, V., Ramos, M.S., Lelievre, F., Barbier-Brygoo, H., Krieger-Liszka, A., Kramer, U., and Thomine, S. (2010). Export of vacuolar manganese by AtNRAMP3 and AtNRAMP4 is required for optimal photosynthesis and growth under manganese deficiency. *Plant Physiol* 152, 1986-1999.

Pubmed: [Author and Title](#)

CrossRef: [Author and Title](#)

Google Scholar: [Author Only Title Only Author and Title](#)

Lanquar, V., Lelievre, F., Bolte, S., Hames, C., Alcon, C., Neumann, D., Vansuyt, G., Curie, C., Schroder, A., Kramer, U., Barbier-Brygoo, H., and Thomine, S. (2005). Mobilization of vacuolar iron by AtNRAMP3 and AtNRAMP4 is essential for seed germination on low iron. *Embo J* 24, 4041-4051.

Pubmed: [Author and Title](#)

CrossRef: [Author and Title](#)

Google Scholar: [Author Only Title Only Author and Title](#)

Lin, Y.T., Hoang, H., Hsieh, S.I., Rangel, N., Foster, A.L., Sampayo, J.N., Lithgow, G.J., and Srinivasan, C. (2006). Manganous ion supplementation accelerates wild type development, enhances stress resistance, and rescues the life span of a short-lived *Caenorhabditis elegans* mutant. *Free Radic Biol Med* 40, 1185-1193.

Pubmed: [Author and Title](#)

CrossRef: [Author and Title](#)

Google Scholar: [Author Only Title Only Author and Title](#)

Luk, E., Carroll, M., Baker, M., and Culotta, V.C. (2003). Manganese activation of superoxide dismutase 2 in *Saccharomyces cerevisiae* requires MTM1, a member of the mitochondrial carrier family. *Proc Natl Acad Sci U S A* 100, 10353-10357.

Pubmed: [Author and Title](#)

CrossRef: [Author and Title](#)

Google Scholar: [Author Only Title Only Author and Title](#)

Luk, E.E., and Culotta, V.C. (2001). Manganese Superoxide Dismutase in *Saccharomyces cerevisiae* Acquires Its Metal Co-factor through a Pathway Involving the Nramp Metal Transporter, Smf2p. *J Biol Chem* 276, 47556-47562.

Pubmed: [Author and Title](#)

CrossRef: [Author and Title](#)

Google Scholar: [Author Only Title Only Author and Title](#)

Marschner, H., Romheld, V., and Kissel, M. (1986). Different strategies in higher plants in mobilization and uptake of iron. *J. Plant Nutr.* 9, 3-7.

Pubmed: [Author and Title](#)

CrossRef: [Author and Title](#)

Google Scholar: [Author Only Title Only Author and Title](#)

Martiniere, A., Bassil, E., Jublanc, E., Alcon, C., Reguera, M., Sentenac, H., Blumwald, E., and Paris, N. (2013). In vivo intracellular pH measurements in tobacco and Arabidopsis reveal an unexpected pH gradient in the endomembrane system. *Plant Cell* 25, 4028-4043.

Pubmed: [Author and Title](#)

CrossRef: [Author and Title](#)

Google Scholar: [Author Only Title Only Author and Title](#)

McNaughton, R.L., Reddi, A.R., Clement, M.H., Sharma, A., Barnese, K., Rosenfeld, L., Gralla, E.B., Valentine, J.S., Culotta, V.C., and Hoffman, B.M. (2010). Probing in vivo Mn²⁺ speciation and oxidative stress resistance in yeast cells with electron-nuclear double resonance spectroscopy. *Proc Natl Acad Sci U S A* 107, 15335-15339.

Pubmed: [Author and Title](#)

CrossRef: [Author and Title](#)

Google Scholar: [Author Only Title Only Author and Title](#)

Mills, R.F., Doherty, M.L., Lopez-Marques, R.L., Weimar, T., Dupree, P., Palmgren, M.G., Pittman, J.K., and Williams, L.E. (2008). ECA3, a Golgi-localized P2A-type ATPase, plays a crucial role in manganese nutrition in Arabidopsis. *Plant Physiol* 146, 116-128.

Pubmed: [Author and Title](#)

CrossRef: [Author and Title](#)

Google Scholar: [Author Only Title Only Author and Title](#)

Milner, M.J., Seamon, J., Craft, E., and Kochian, L.V. (2013). Transport properties of members of the ZIP family in plants and their role in Zn and Mn homeostasis. *J Exp Bot* 64, 369-381.

Pubmed: [Author and Title](#)

CrossRef: [Author and Title](#)

Google Scholar: [Author Only Title Only Author and Title](#)

Momonoi, K., Yoshida, K., Mano, S., Takahashi, H., Nakamori, C., Shoji, K., Nitta, A., and Nishimura, M. (2009). Avacuolar iron transporter in tulip, TgVit1, is responsible for blue coloration in petal cells through iron accumulation. *Plant J* 59, 437-447.

Pubmed: [Author and Title](#)

CrossRef: [Author and Title](#)

Google Scholar: [Author Only Title Only Author and Title](#)

Nelson, N., Sacher, A., and Nelson, H. (2002). The significance of molecular slips in transport systems. *Nat Rev Mol Cell Biol* 3, 876-881.

Pubmed: [Author and Title](#)

CrossRef: [Author and Title](#)

Google Scholar: [Author Only Title Only Author and Title](#)

Nevo, Y., and Nelson, N. (2006). The NRAMP family of metal-ion transporters. *Biochim Biophys Acta* 1763, 609-620.

Pubmed: [Author and Title](#)

CrossRef: [Author and Title](#)

Google Scholar: [Author Only Title Only Author and Title](#)

Nickelsen, J., and Rengstl, B. (2013). Photosystem II assembly: from cyanobacteria to plants. *Annu Rev Plant Biol* 64, 609-635.

Pubmed: [Author and Title](#)

CrossRef: [Author and Title](#)

Google Scholar: [Author Only Title Only Author and Title](#)

Pedas, P., Schiller Stokholm, M., Hegelund, J.N., Ladegard, A.H., Schjoerring, J.K., and Husted, S. (2014). Golgi localized barley MTP8 proteins facilitate Mn transport. *PLoS One* 9, e113759.

Pubmed: [Author and Title](#)

CrossRef: [Author and Title](#)

Google Scholar: [Author Only Title Only Author and Title](#)

Peiter, E., Montanini, B., Gobert, A., Pedas, P., Husted, S., Maathuis, F.J., Blaudez, D., Chalot, M., and Sanders, D. (2007). A secretory pathway-localized cation diffusion facilitator confers plant manganese tolerance. *Proc Natl Acad Sci U S A* 104, 8532-8537.

Pubmed: [Author and Title](#)

CrossRef: [Author and Title](#)

Google Scholar: [Author Only Title Only Author and Title](#)

Pittman, J.K., Shigaki, T., Marshall, J.L., Morris, J.L., Cheng, N.H., and Hirschi, K.D. (2004). Functional and regulatory analysis of the *Arabidopsis thaliana* CAX2 cation transporter. *Plant Mol Biol* 56, 959-971.

Pubmed: [Author and Title](#)

CrossRef: [Author and Title](#)

Google Scholar: [Author Only Title Only Author and Title](#)

Portnoy, M.E., Liu, X.F., and Culotta, V.C. (2000). *Saccharomyces cerevisiae* expresses three functionally distinct homologues of the nramp family of metal transporters. *Mol. Cell. Biol.* 20, 7893-7902.

Pubmed: [Author and Title](#)

CrossRef: [Author and Title](#)

Google Scholar: [Author Only Title Only Author and Title](#)

Ravet, K., Touraine, B., Kim, S.A., Cellier, F., Thomine, S., Guerinot, M.L., Briat, J.F., and Gaymard, F. (2009). Post-translational regulation of AtFER2 ferritin in response to intracellular iron trafficking during fruit development in *Arabidopsis*. *Mol Plant* 2, 1095-1106.

Pubmed: [Author and Title](#)

CrossRef: [Author and Title](#)

Google Scholar: [Author Only Title Only Author and Title](#)

Roth, J.A. (2006). Homeostatic and toxic mechanisms regulating manganese uptake, retention, and elimination. *Biol Res* 39, 45-57.

Pubmed: [Author and Title](#)

CrossRef: [Author and Title](#)

Google Scholar: [Author Only Title Only Author and Title](#)

Rudolph, H.K., Antebi, A., Fink, G.R., Buckley, C.M., Dorman, T.E., LeVitre, J., Davidow, L.S., Mao, J.I., and Moir, D.T. (1989). The yeast secretory pathway is perturbed by mutations in PMR1, a member of a Ca²⁺ ATPase family. *Cell* 58, 133-145.

Pubmed: [Author and Title](#)

CrossRef: [Author and Title](#)

Google Scholar: [Author Only Title Only Author and Title](#)

Sasaki, A., Yamaji, N., Yokosho, K., and Ma, J.F. (2012). Nramp5 is a major transporter responsible for manganese and cadmium uptake in rice. *Plant Cell* 24, 2155-2167.

Pubmed: [Author and Title](#)

CrossRef: [Author and Title](#)

Google Scholar: [Author Only Title Only Author and Title](#)

Schmidt, S.B., Jensen, P.E., and Husted, S. (2016). Manganese Deficiency in Plants: The Impact on Photosystem II. *Trends Plant Sci* 21,

622-632.

Pubmed: [Author and Title](#)

CrossRef: [Author and Title](#)

Google Scholar: [Author Only Title Only Author and Title](#)

Schneider, A., Steinberger, I., Herdean, A., Gandini, C., Eisenhut, M., Kurz, S., Morper, A., Hoecker, N., Ruhle, T., Labs, M., Flugge, U.I., Geimer, S., Schmidt, S.B., Husted, S., Weber, A.P., Spetea, C., and Leister, D. (2016). The Evolutionarily Conserved Protein PHOTOSYNTHESIS AFFECTED MUTANT71 Is Required for Efficient Manganese Uptake at the Thylakoid Membrane in Arabidopsis. *Plant Cell* 28, 892-910.

Pubmed: [Author and Title](#)

CrossRef: [Author and Title](#)

Google Scholar: [Author Only Title Only Author and Title](#)

Su, Z., Chai, M.F., Lu, P.L., An, R., Chen, J., and Wang, X.C. (2007). AtMTM1, a novel mitochondrial protein, maybe involved in activation of the manganese-containing superoxide dismutase in Arabidopsis. *Planta* 226, 1031-1039.

Pubmed: [Author and Title](#)

CrossRef: [Author and Title](#)

Google Scholar: [Author Only Title Only Author and Title](#)

Supek, F., Supekova, L., Nelson, H., and Nelson, N. (1996). A yeast manganese transporter related to the macrophage protein involved in conferring resistance to mycobacteria. *Proc. Natl Acad. Sci. U. S. A.* 93, 5105-5110.

Pubmed: [Author and Title](#)

CrossRef: [Author and Title](#)

Google Scholar: [Author Only Title Only Author and Title](#)

Tanaka, T., Tanaka, H., Machida, C., Watanabe, M., and Machida, Y. (2004). A new method for rapid visualization of defects in leaf cuticle reveals five intrinsic patterns of surface defects in Arabidopsis. *Plant J* 37, 139-146.

Pubmed: [Author and Title](#)

CrossRef: [Author and Title](#)

Google Scholar: [Author Only Title Only Author and Title](#)

Techau, M.E., Valdez-Taubas, J., Popoff, J.F., Francis, R., Seaman, M., and Blackwell, J.M. (2007). Evolution of differences in transport function in Slc11a family members. *J Biol Chem* 282, 35646-35656.

Pubmed: [Author and Title](#)

CrossRef: [Author and Title](#)

Google Scholar: [Author Only Title Only Author and Title](#)

Thomine, S., Wang, R., Ward, J.M., Crawford, N.M., and Schroeder, J.I. (2000). Cadmium and iron transport by members of a plant metal transporter family in Arabidopsis with homology to Nramp genes. *Proc. Natl Acad. Sci. U. S. A.* 97, 4991-4996.

Pubmed: [Author and Title](#)

CrossRef: [Author and Title](#)

Google Scholar: [Author Only Title Only Author and Title](#)

Uemura, T., and Nakano, A. (2013). Plant TGNs: dynamics and physiological functions. *Histochem Cell Biol* 140, 341-345.

Pubmed: [Author and Title](#)

CrossRef: [Author and Title](#)

Google Scholar: [Author Only Title Only Author and Title](#)

Whittaker, M.M., Penmatsa, A., and Whittaker, J.W. (2015). The Mtm1p carrier and pyridoxal 5'-phosphate cofactor trafficking in yeast mitochondria. *Arch Biochem Biophys* 568, 64-70.

Pubmed: [Author and Title](#)

CrossRef: [Author and Title](#)

Google Scholar: [Author Only Title Only Author and Title](#)

Wilson, D.O., Boswell, F.C., Ohki, K., Parker, M.B., Shuman, L.M., and Jellum, M.D. (1982). Changes in soybean seed oil and protein as influenced by manganese nutrition. *Crop Science* 22, 948-952.

Pubmed: [Author and Title](#)

CrossRef: [Author and Title](#)

Google Scholar: [Author Only Title Only Author and Title](#)

Wu, Z., Liang, F., Hong, B., Young, J.C., Sussman, M.R., Harper, J.F., and Sze, H. (2002). An endoplasmic reticulum-bound Ca(2+)/Mn(2+) pump, ECA1, supports plant growth and confers tolerance to Mn(2+) stress. *Plant Physiol* 130, 128-137.

Pubmed: [Author and Title](#)

CrossRef: [Author and Title](#)

Google Scholar: [Author Only Title Only Author and Title](#)

Yang, M., Cobine, P.A., Molik, S., Naranuntarat, A., Lill, R., Winge, D.R., and Culotta, V.C. (2006). The effects of mitochondrial iron homeostasis on cofactor specificity of superoxide dismutase 2. *Embo J* 25, 1775-1783.

Pubmed: [Author and Title](#)

CrossRef: [Author and Title](#)

Google Scholar: [Author Only Title Only Author and Title](#)

Yeats, T.H., and Rose, J.K. (2013). The formation and function of plant cuticles. *Plant Physiol* 163, 5-20.

Pubmed: [Author and Title](#)

CrossRef: [Author and Title](#)

Google Scholar: [Author Only Title Only Author and Title](#)

Zhang, Y., Xu, Y.H., Yi, H.Y., and Gong, J.M. (2012). Vacuolar membrane transporters OsVIT1 and OsVIT2 modulate iron translocation between flag leaves and seeds in rice. Plant J 72, 400-410.

Pubmed: [Author and Title](#)

CrossRef: [Author and Title](#)

Google Scholar: [Author Only Title Only Author and Title](#)

**Intracellular Distribution of Manganese by the Trans-Golgi Network Transporter NRAMP2 is
Critical for Photosynthesis and Cellular Redox Homeostasis**

Santiago Alejandro, Rémy Cailliatte, Carine Alcon, Léon Dirick, Frédéric Domergue, David Correia,
Loren Castaings, Jean-François Briat, Stéphanie Mari and Catherine Curie

Plant Cell; originally published online November 27, 2017;
DOI 10.1105/tpc.17.00578

This information is current as of January 15, 2018

Supplemental Data	/content/suppl/2017/11/27/tpc.17.00578.DC1.html /content/suppl/2017/12/20/tpc.17.00578.DC2.html
Permissions	https://www.copyright.com/ccc/openurl.do?sid=pd_hw1532298X&issn=1532298X&WT.mc_id=pd_hw1532298X
eTOCs	Sign up for eTOCs at: http://www.plantcell.org/cgi/alerts/ctmain
CiteTrack Alerts	Sign up for CiteTrack Alerts at: http://www.plantcell.org/cgi/alerts/ctmain
Subscription Information	Subscription Information for <i>The Plant Cell</i> and <i>Plant Physiology</i> is available at: http://www.aspb.org/publications/subscriptions.cfm